Optimisation of femoral osteotomies around the knee using the finite element method

TU Delft

UMC Utrecht

Reijan Joël van der Weijde
4729358
27-03-2024

Optimisation of femoral osteotomies around the knee using the finite element method

In partial fullfillment of the requirments for the degree of

Master of science
in biomedical engineering

Daily supevisors:
Joëll Magre
Chien Nguyen

Thesis comittee:
Prof. dr. ir. H.H. Weinans
Nazli Tümer
Chien Nguyen

TU Delft

UMC Utrecht

Abstract

Introduction

Osteoarthritis (OA) is a prevalent joint disease affecting 7% of the global population in 2020. Lower limb malalignment emerges as a significant contributor to OA, presenting as varus or valgus misalignment. This deviation induces unicompartmental pathology, leading to the wear and tear of the protective cartilage. Surgical interventions, including osteotomies, are essential in managing unicompartmental knee OA. During osteotomies, hinge fractures are a common complication.

This paper focuses on optimizing open wedge osteotomies, specifically exploring complications in medial open wedge distal femoral osteotomy (DFO) using finite element models. And investigates the viability of the medial open wedge DFO compared to the lateral open wedge DFO.

Method

The research employed a systematic approach to investigate ways to avoid hinge fractures in Distal Femoral Osteotomy (DFO). Finite Element Modelling (FEM) served as the cornerstone of our methodology, providing a numerical solution. The process involved the creation of finite element models from CT scans through the subdivision of femoral geometry. The automated generation of these models was facilitated by a combination of 3-matic, Mimics, and Abaqus. Using Python scripting in these different programs, a workflow for model creation and parameter variation was created. The lateral open wedge DFO model, serving as the baseline, underwent systematic alterations to explore the impact of hinge size, osteotomy gap angle, and other variables. The creation of finite element models involved several key steps, including geometry creation, mesh generation, addition of material properties, and the application of boundary and loading conditions. Material properties were assigned based on a simplified isotropic model derived from Hounsfield units. Extra attention was given to automate the process of model generation to ensure efficiency and reproducibility.

Results

Six distinct models were created with a comprehensive analysis of their attributes and shortcomings. The study finds that the medial open wedge DFO does not induce hinge tension. Comparative analyses in both opening and loading stages reveal nuanced stress and strain differences with the lateral open wedge DFO. No clear conclusion can be given as to the viability of the medial open wedge DFO compared to the lateral open wedge DFO. In-depth exploration indicates that smaller hinges are favourable for osteotomy gap opening, while larger hinges (10mm and above) contribute to stability during loading. Minimal impact on stress concentration is observed for osteotomy gap angle variations. The study explores the effectiveness of drill holes in stress relief, highlighting precision challenges.

Discussion

Acknowledging inherent limitations such as partial volume effects and assumptions about material properties. The study suggests promising avenues for future research. Recommendations for future research include in vivo experiments, exploration of XFEM and fracture mechanics, and further refinement of modelling techniques. This study provides nuanced insights into hinge fractures during open wedge DFO, guiding future research and bridging the gap between finite element modelling and clinical realities.

Table of Contents

Table of Figures

Table of Tables

1. Introduction

Osteoarthritis (OA) is the most common joint disease worldwide, affecting approximately 7% of the people in 2020[1]. OA is a multi-factorial degenerative joint disorder causing pain and disability, which can severely impact an individual's life. This disease is characterized by the wear of the protective cartilage of the joints. The rapid increase in OA incidence suggests that the disease will have a growing impact on the healthcare system, partly due to the aging population and increasing obesity rate which are both risk factors for OA[1].

1.1. Varus and valgus

One of the inducers and progressors of knee OA is lower limb malalignment, either varus (O-type legs) or valgus (X-type legs) as can be seen in FIGURE 1, causing unicompartmental pathology in which one side is overloaded causing wear and tear.

In the case of a lower limb malalignment the mechanical axis is not optimal the mechanical axis in the knee joint is too much oriented to the medial side (varus) or to the lateral side (valgus). The mean stance, in healthy adults, is slightly in varus ranging from 1 to 2 degrees [2].

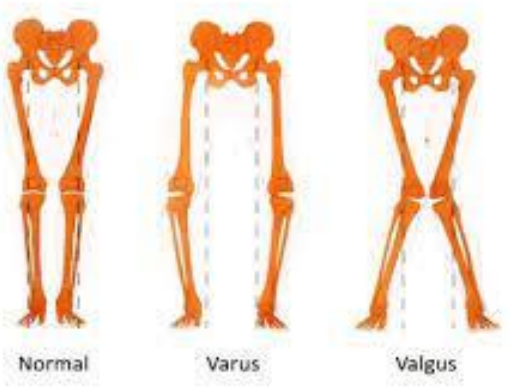

FIGURE 1. VARUS AND VALGUS STANCE COMPARED TO NORMAL [52]

In most cases approximately 60% of the weight bearing force is transferred through the medial compartment and 40% through the lateral compartment. In case of a varus or valgus stance (FIGURE 1) the affected compartment is overloaded. This can lead to the development or progression of unicompartimental knee OA, where only one side of the knee (medial in case of varus or lateral in case of valgus) is affected while the other compartment remains unaffected [3].

1.2. Treatment

The treatment of unicompartimental knee OA can be done with surgical and non-surgical options. If OA is not too advanced, first non-surgical options are considered. These include using a brace, lifestyle changes to alleviate the joints, pain relief medication, and intraarticular injections. If this does not provide the desired improvement or the patient is not able to adapt their lifestyle, surgical options may be necessary. There are three main surgical treatments for unicompartimental knee OA: unicompartmental knee arthroplasty, total knee arthroplasty and osteotomy[6].

In recent years, there is an increasing awareness that biological preservation of the knee is of great importance, meaning putting more emphasis on conservative treatments such as an osteotomy. Therefore, early detection of symptoms is important in order to preserve the knee while there is still regenerative ability left. This can be especially important in young and active patients [7][8][9].

1.3. Osteotomy and hinge fractures

This thesis will focus on hinge fractures in open wedge osteotomies. And utilize finite element models to predict the outcomes by incorporating various parameters.

For a stable osteotomy an intact bone bridge or hinge is required. This means that a small part of the opposite cortical bone will not be cut but stays intact, while the surgeon opens the osteotomy gap. As bone behaves somewhat plastic, the bone will not break fully but functions as a hinge. However, there is a risk that the hinge will fail, either during the opening of the gap, or later when the patient starts walking and mechanically loading the bone.

A surgical osteotomy can result in several complications. The most common complications are: hinge fractures (HF), under or over correction, hardware failure, regional pain syndrome, delayed and non-union, neurovascular damages, and infection [10].

HFs are divided into three classifications [11] (Figure 2 and Figure 3), with different definitions for the distal femoral and proximal tibial osteotomies [12] (Figure 3). For a high tibial osteotomy (HTO) type I the fracture extends in line with the osteotomy cut, type II fractures away from the tibiofemoral joint, and type III fractures towards the tibiofemoral joint compromising the tibial plateau (Figure 5). In DFO HF type I goes along the osteotomy cut, type III goes superior, and type II goes inferior (Figure 2).

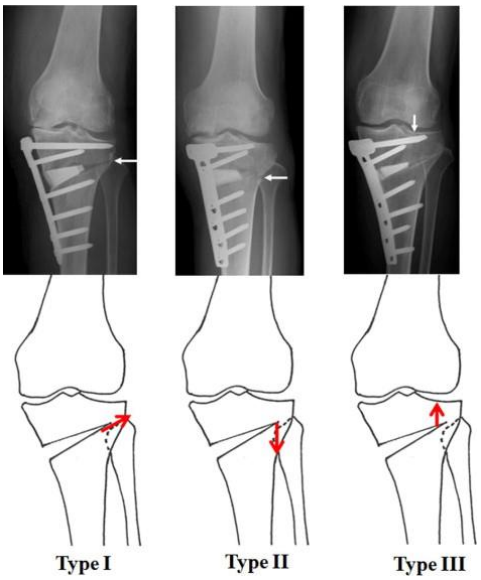

Figure 2. Classifications for HTO[13]

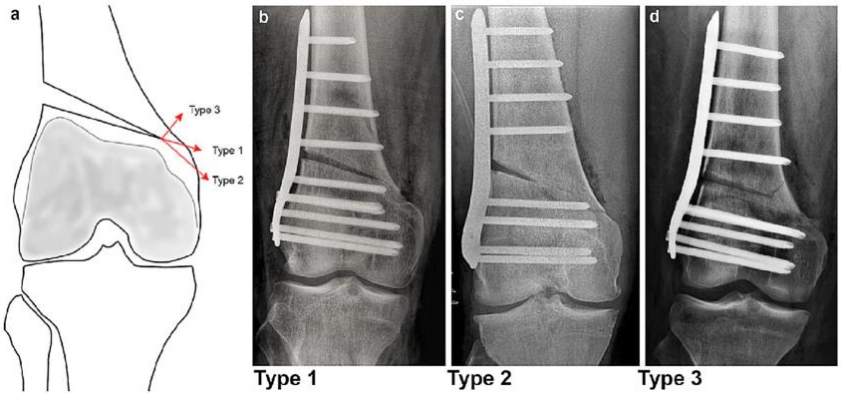

Figure 3. Classifications for hinge fractures LOWFO[12]

Type I fractures are usually stable (the bone does not move) in both HTO and DFO, and does not show excessive micromotion. Research indicates that type II and III fractures are unstable[14][13][15] and pose a risk for micromotion, excessive micromotion can impede bone healing[16]. Type II and III fractures delay rehabilitation due to an extended non-weight bearing regime[17]. Additional revision

surgery or additional plate fixation are necessary if the HF eventually leads to a non-union. The incidence of hinge fractures depends on factors such as the chosen osteotomy technique, patient characteristics, and the size of the osteotomy gap, typically ranging between 15% and 30%[18].

A novel surgical technique involves introducing a K-wire through the hinge to enhance its torsional stiffness is a novel surgical technique, which has demonstrated a reduction in hinge fractures [19].

1.4. Problem statement

Patients with a leg length discrepancy and indicated for a valgus producing femoral osteotomy, are best helped with an open wedge medial

osteotomy. This technique is also advantageous in terms of complexity and surgical accuracy. The open wedge technique also has the advantage of being surgically less complex. This method has not been widely reported in literature to the best of our knowledge.

The open wedge medial DFO approach was utilized in five cases at the University Medical Centre Utrecht, with the hinge placement based on the medial closed wedge DFO technique[20]. Regrettably, four out of five surgeries resulted in complications, three of which led to hinge fractures: two of type III and one of type I. This notably high complication rate warrants further investigation. In contrast, lateral closed wedge DFO and lateral open wedge DFO are widely accepted procedures[8], , with significantly lower complication rates, particularly for unstable hinge fractures.

The primary objective of this research is to investigate the cause of hinge fractures in medial open wedge DFO. Our current hypothesis posits that, due to the curvature in the frontal plane of the femur, the hinge of the medial open wedge DFO is subjected to tension, whereas in lateral open wedge DFO, the hinge experiences compression. Compressive forces facilitate bone healing, whereas tension does not yield the same beneficial effects[21]. Over time, this tension could lead to escalating damage in the hinge before bone recovery[22].

Several secondary goals have also been identified during the writing of this paper:

- Investigating if the entry point and thickness of the hinge have an effect on the way an osteotomy should be performed, both for the operation and rehabilitation.
- Additionally, exploring the potential of a drill hole perpendicular to the osteotomy plane to reduce stress and strain concentrations, thereby mitigating hinge fractures during osteotomies. This solution has been proposed in multiple papers [23][24][25], albeit its implementation currently necessitates a more invasive surgery.
- As mentioned earlier, fractures are theorized to occur at two stages: during the osteotomy itself and when the patient begins to use the affected limb again.

2. Materials and Methods

This chapter addresses the methodology for investigating the questions posed in the problem statement. This will be achieved through the application of the finite element method in this thesis to examine the issues outlined in the problem statement. The investigation will involve the following models:

- A Lateral open wedge DFO and medial open wedge DFO
    - To investigate the difference between a lateral and medial open wedge DFO
- A lateral open wedge DFO with different hinge sizes
    - To investigate the ideal hinge size
- A lateral open wedge DFO with a different entry point for the hinge
    - To investigate the effect of different entry points and resulting different angle of the osteotomy plane
- A lateral open wedge DFO with drill holes and without
    - To compare the difference between the model with and without drill holes
- Unaltered model

The unaltered model is used to create an impression of the normal force distribution in the femur and validate the model by comparing it with other models from published papers.

In all the models, there are two potential moments when a fracture could occur: during the osteotomy procedure or when the patient begins to use the affected limb again by applying force to it. Both of these scenarios will be modelled for each of the aforementioned points, except for the unaltered model.

These models will serve to address the primary and secondary objectives of this thesis. The methods for creating and utilizing these models are detailed in this chapter. Firstly, a general explanation of model creation will be provided, followed by an explanation of how these models are automated. Subsequently, information about each specific model will be presented

2.1. Background

An osteotomy is a complex invasive procedure comprising multiple steps, each presenting potential complications. These moments include the following:

The initial moment occurs during the opening of the osteotomy gap, which is essential for achieving the desired correction. This process exerts considerable stress and strain on the bone, particularly in and around the hinge, which has been documented to increase the risk of fractures, especially with larger corrections[12][29].

The second moment where a hinge fracture could occur is when the patient resumes daily activities. Patients are permitted to apply partial pressure on the leg a few days after the operation. However, due to the removal of bone, the force is dispersed over a much smaller area, as illustrated in Figure 4.

To identify the issues that arise during and after osteotomies, both of these scenarios are modelled. Throughout the remainder of this thesis, the opening of the osteotomy gap will be referred to as state 1, while the loading of the completed osteotomy will be referred to as state 2.

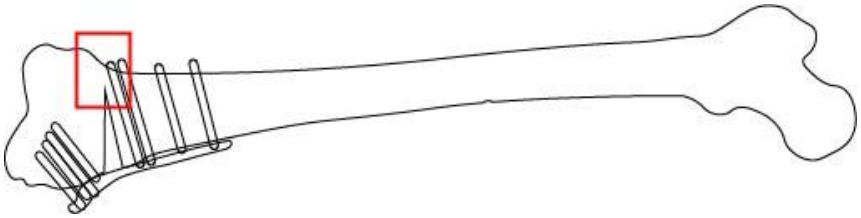

Figure 4. Location of possible stress concentrations due to removed material

2.2. Creation of the finite element models

Finite element modelling (FEM) is a numerical method used for solving differential equations in 2D or 3D spaces. This is accomplished by discretizing the geometry using a mesh, which subdivides the geometry into smaller elements called finite elements. As these elements have a finite number of points, equations can be formulated for each element. These equations are then assembled into a larger system of equations that represents the entire femur. Therefore, FEM approximates the solution by simplifying the geometry into a finite number of points. The primary advantage of FEM is its ability to simulate situations that would typically be too invasive or difficult to measure. Given that both the angle of the osteotomy gap and the hinge size will necessitate multiple models, an attempt will be made to automate the modelling process. This will not only provide insight into the feasibility of creating automated patient-specific finite element models but also ensure the elimination of any unwanted differences between models.

This chapter elucidates the process of creating Finite Element Models[30]. To create each model, the following steps were taken in chronological order:

1. Creation of the geometry
2. Creation of the Mesh
3. Adding material properties
4. Boundary and loading conditions
5. Explanation of specific models.

Although the operations may vary slightly as each model is designed to provide different information, the steps remain similar across all models.

For all models, an osteotomy gap opening of 10 mm was selected. This correction was chosen based on the consensus from various papers indicating that corrections of 10 mm and larger result in a significant increase in HF as was found in the literature study that predates this thesis.

2.3. Geometry

This subchapter will focus on the creation of the shape used for the models. It is divided into three parts: a general overview of creating a 3D model of a femur, followed by explanations of the geometries for state 1 and state 2. To create the geometry of the femur, a CT scan from a healthy patient was utilized. The DICOM files from the CT scan (GE LightSpeed VCT; General Electric Healthcare, Chalfont, St Giles, UK; 120 kVp, 100 mA; slice thickness of 0.7 mm) were imported into Mimics. Subsequently, 3-matic software was employed to modify the geometry for osteotomy. In-house developed scripts for 3-matic were used to define the femur's landmarks, ensuring they fell within normal ranges (refer to Table 1). Additionally, this software was utilized to define the different planes of the femur for later use.

Table 1. Showing the measurements of the femur used in this research

LPFA	88.10
mLDFA	87.04
Femoral anteversion	0.62

State 1: Making the incision

In collaboration with surgeons from UMC Utrecht, we identified optimal cutting planes for both medial and lateral open wedge DFO procedures. These planes were offset from the femur's transverse plane, delineated by the intercondylar fossa (illustrated in Figure 5 with the green line). This offset was determined based on the positioning of the hinge and saw insertion point.

For the hinge, we located the most medial point in the coronal plane and then shifted it laterally by 10 mm to establish the hinge position. Similarly, for the saw insertion point, we identified the most lateral point in the coronal plane. These two points, along with the femur's coronal plane, were utilized to create a new plane perpendicular to the coronal plane and passing through both points. This plane was extended by 1.2 mm, corresponding to the oscillating saw blade used during osteotomies. Specific locations and distances are illustrated in Figure 5 and detailed in Table 2.

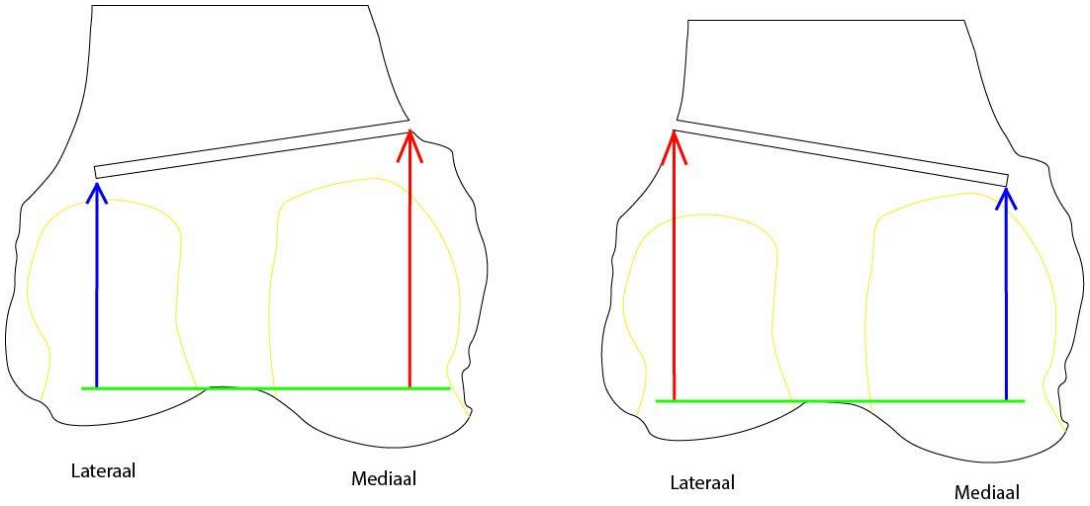

Figure 5. both the medial open wedge DFO(left) and lateral open wedge DFO(right) where the incision location is blue and the blue line is the hinge. The green line is the zero-point location

Table 2. The distance between the hinge location and saw location incision.

	Media open wedge DFO	Lateral open wedge DFO
Hinge location	34.76 mm	43.89 mm
Location of the saw incision	36.79 mm	48.26 mm

State 2: creating the wedge

To create the geometry of the bone with the wedge, the deformed geometry of the bone with the osteotomy is utilized. This geometry is exported from the finalized model with the osteotomy and imported into a new model where the wedge in the bone is created.

For the geometry of the plates, 3D models were readily available. Commercially available plates were utilized for the lateral open wedge DFO. However, for medial open wedge DFO, no specialized plate is available. Therefore, the lateral closed wedge DFO plate, which is commercially available, was utilized. The placements of the plates were done in cooperation with the orthopaedic surgeons of the UMC Utrecht. Screws are normally used to fix the plate to the bone, which are inserted bi-cortical. Because of technical difficulties the decision was made to consider the interaction between the plate and bone as fully bonded and discarding the screws itself.

2.4. Mesh

In a finite element model, larger objects are divided into smaller elements to enable calculations. The areas of interest are meshed with relatively small elements (many nodes), while less critical areas are meshed with larger elements to reduce calculation time. The way and reasons for the choice of meshing will be explained in this chapter.

Mesh dependency:

For both the mesh convergence and mesh dependency a lateral open wedge DFO model was used with a hinge of 10 mm and a osteotomy angle of 15 degrees.

To assess the mesh dependency of all the models, a control in Abaqus was conducted for each created model to ensure that elements fell within the expected range. Ideally, uniformity among elements is preferred. This is however not possible due to the geometry. The shape factor, indicating how well-formed elements are, was set with a strict threshold of 0.0001. We also limited corner angles to be less than 5 degrees and more than 170 degrees, excluding elements with extreme angles for better geometric stability. An aspect ratio greater than 10 was required to maintain balanced proportions and avoid numerical issues. Despite these specific criteria, no errors were observed in any models, confirming the effectiveness of these conditions in producing dependable and accurate results in finite element analysis.

State 1:

The region of interest lies around the hinge and above, where the greatest stress and strain concentrations are observed in both moment 1 and moment 2 (refer to Figure 6). This segmentation was achieved using the 3-matic tool to mesh regional areas differently. The chosen area is outlined from the proximal frontal corner of the osteotomy gap. A box is created 10 mm above, 5 mm below through the entire femur in the transverse direction and in the medial direction until the cortex. In this area hinge fractures are most common and the highest forces are expected. This means this area is of more interest then it's surroundings. This box is also visualised in Figure 6.

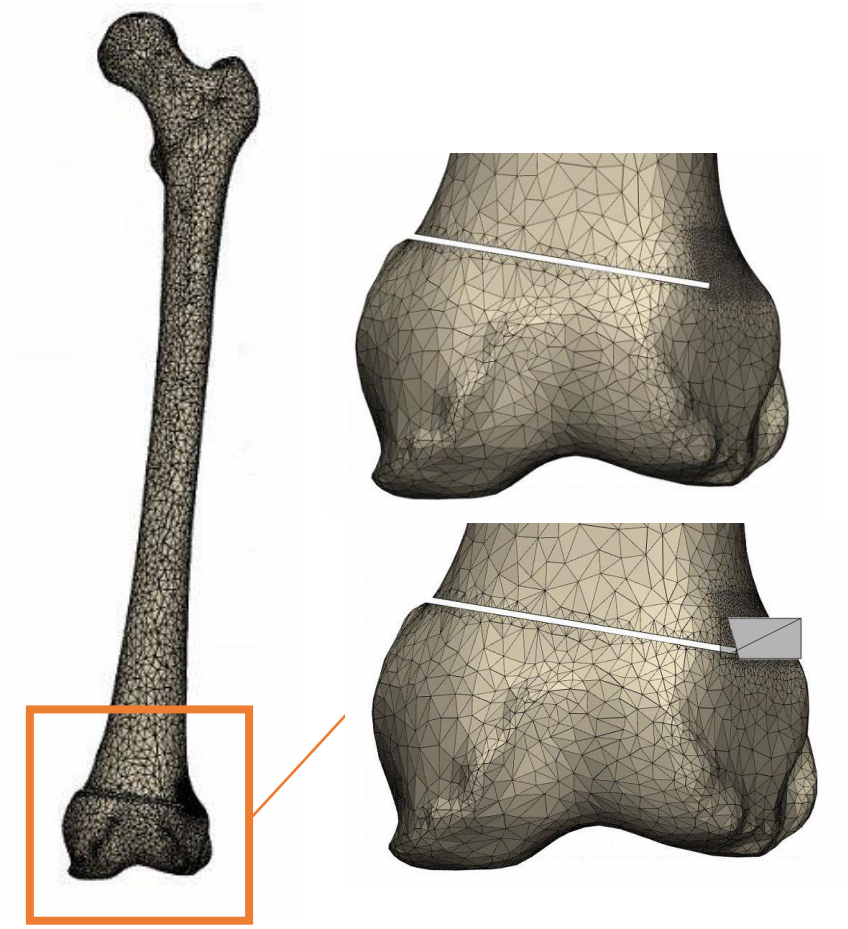

Figure 6. The mesh of the model with a box that shows the more concentrated mesh at the hinge location

In total the models consist of 200.000 to 400.000 elements, depending on the hinge size. An example can be seen in Table 3 where the hinge size and number of elements are displayed.

Table 3. Showing the different amounts of elements based on the hinge size of the model

Hinge size	Elements
5 mm	207921
7.5 mm	243746
10 mm	283720
12.5 mm	327699
15 mm	373162

In 3-matic, a 3D modelling and design software developed by Materialise, the following settings are employed to create these elements: 1.75 mm elements for the fine mesh and 3 mm elements for the general mesh. C3D10 elements were selected. This type was selected because tetrahedrons were the only available option in 3-matic. A quadratic (C3D10) approach was preferred over a linear (C3D4) approach due to the complex geometry and anticipated deformations. Furthermore, a mesh independence analysis was conducted to evaluate the model's mesh dependency.

State 2:

Moment 2 is a continuation of moment 1, signifying that the deformed mesh at the end of moment 1 serves as the starting point for state 2.

The plates for the medial open wedge DFO were modelled using the same C3D10 elements. A total of 3451 elements were utilized for the medial open wedge DFO, while 2195 elements were used for the lateral open wedge DFO. This decision aimed to maintain the original geometry while minimizing the number of elements. The mesh of the plates was not deemed crucial for the hinge results, as this research primarily focuses on factors other than plate failure.

2.5. Material properties

Assigning material properties to the created elements is the subsequent step in the model creation process. This chapter elucidates the incorporation of material properties.

Bone is a complex non uniform anisotropic material[31], posing challenges for accurate simulation. To simplify a isotropic material was chosen To simplify, an isotropic material model was chosen. Material non-uniformity was simulated using Hounsfield units, with material properties derived from density. This method, validated in literature, establishes relationships between Hounsfield units, density, and Young's modulus.[32][33].

State 1:

Various methods exist to establish the correlation between Hounsfield units, density, and Young's modulus. In this case, an in vivo study was chosen to validate previously developed formulas. Carranza et al. conducted experiments involving osteotomies on cadaver tibias, comparing outcomes with simulated models to validate material properties. Alignment between experimental and simulated deformations ensures accurate representation. While Carranza et al. focused on tibias, the correlation between Hounsfield units and femur density is similar. Formulas translating Hounsfield units to density and Young's modulus are provided in Formulas 1 and 2, with a Poisson's ratio assumed as 0.3 for the entire bone.[26].

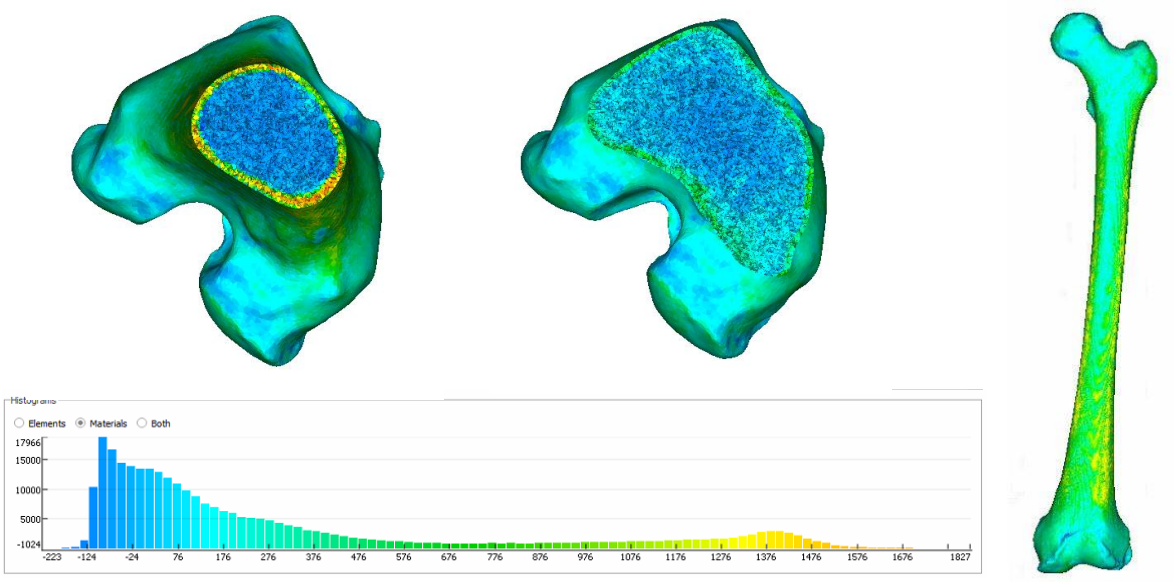

Figure 7. The material distribution throughout the femur without any alterations. In the top left corner, the two figures show a mesh density that is only available in the hinge due to calculation limitations.

As depicted in Figure 7, two peaks are observed in the material distribution, with a total of 100 different material classes created. Experimental tests indicated that fewer classes would result in a less accurate fit of the curve, while more classes would lead to larger file sizes. These peaks represent both trabecular and cortical bone, with the peak on the right corresponding to cortical bone. Cortical bone is predominantly located along the femur's cortex, as expected.

As described, the location of elements is correlated with Hounsfield units. The formulas used to convert Hounsfield units to density and Young's modulus are provided below.

$$\rho = 1 + 0.0007185 * \text{HU in g}/cm^2 \text{ [34]}$$

Formula 1

$$\text{E} = 4778\rho^{1.99} \text{ [35]}$$

Formula 2

State 2:

For state 2, the deformed geometry from state 1 is imported to reuse the mesh. This ensures that the elements retain the same element IDs, facilitating the copying of material properties from state 1.

In state 2, plates are also introduced, with both plates made of Ti-6Al-4V. This material is uniform and isotropic, and simulated accordingly. It is assumed that the material will remain within the elastic region and not reach the yield or ultimate strength. The assigned material properties include a Young's modulus of 114 GPa and a Poisson's ratio of 0.3[36].

2.6. Boundary and loading conditions

The boundary and loading conditions encompass the forces and displacements applied to the models. This section will elucidate these conditions.

State 1:

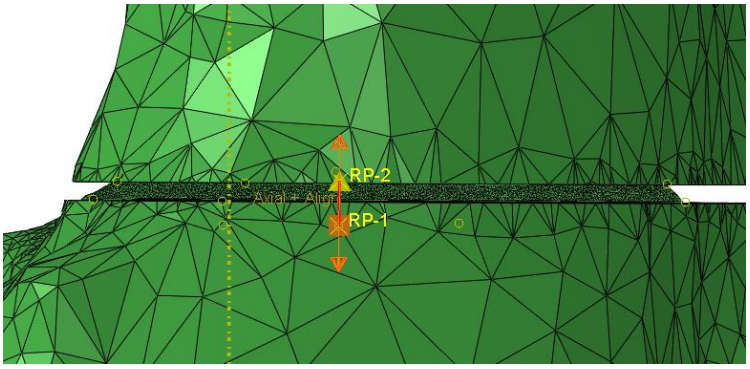

Figure 8. The displacement vector perpendicular to the plane of the osteotomy gap

Opening the osteotomy is akin to inserting a wedge into a gap during surgery. However, the method may vary slightly depending on the instruments used to perform the procedure. While the forces applied are generally similar, they can vary based on the instruments utilized. The majority of the force is concentrated at the location where the wedge is inserted. To closely mimic these forces, two separate node selections were made: one on the distal side of the osteotomy gap and one on the proximal side. Each node set is coupled to a reference point, forming a line perpendicular to the plane of the osteotomy gap, as illustrated in Figure 8. A displacement is then applied between the two reference points along the defined line, simulating the force applied by a wedge or similar action.

Additionally, an area 2.5 times the width of the femur proximal from the osteotomy gap is constrained to prevent interference with results around the hinge.

State 2:

For state 2, a normal gait was simulated to replicate real-world conditions. The loading force and axis were chosen in accordance with Bergmann et al. to simulate the largest stress moment during a normal walk. This force is divided into x, y, and z components and applied to the head of the femur. A reference point, coupled to the loading area, facilitates the application of this force. The loading location is selected based on the findings of Kainz et al[37]. The femur is constrained at the two condyles were the force is typically transferred to the knee[37]. To simulate the interaction between the plate and femur, the surface nodes of the femur are tied to the inside of the screw holes of the plate, thereby modelling the interaction between the femur and plate.

Additional model with screws

In state 2, screws are typically used in vivo to fixate the plate to the femur. However, due to technical limitations in the created models, this fixation was done virtually. An initial test model was created to investigate the visibility of implementing screws in this situation. The details of this model will be further elucidated.

2.7. Models

The primary model, as detailed in Chapter 2.6, is the lateral open wedge DFO model. An identical copy is also created as a medial open wedge DFO model using the same methodology. To explore the impact of differences such as hinge size and osteotomy gap angle, modified models are necessary. All models mentioned below are derived from the model described in Chapter 2, with the changes outlined along with the rationale behind their creation.

Medial open wedge DFO and lateral open wedge DFO

For both the medial and lateral open wedge DFO models, the steps outlined in Chapter 2 were followed. The primary difference in State 1 was the side of the femur being operated on, either lateral or medial. In State 2, a specialized plate was available for the lateral side, while for the medial side, no such specialized plate was available.

For the hinge size 10 mm was taken as it's the industry standard. While the location of the incision was discussed with surgeons and based off their experience.

Hinge size

In the investigation of different hinge sizes, the lateral open wedge DFO model serves as the basis. Multiple models with varying hinge sizes were created. While a 10 mm hinge size is common in the literature, there is no conclusive evidence regarding its ideal size. It is anticipated that a smaller hinge may be preferred during the opening of the osteotomy gap, whereas a larger hinge may be preferred during healing and daily activities. This preference may vary based on the specific properties of the femur.

In collaboration with orthopedic surgeons from UMC Utrecht, it was decided to use increments of 2.5 mm for hinge size variations, as this approximates the precision achievable during surgery. For this research, hinge sizes of 5, 7.5, 10, 12.5, and 15 mm were selected. These variations were implemented in State 1 during the creation of the osteotomy gap, resulting in five different geometries with distinct hinge sizes.

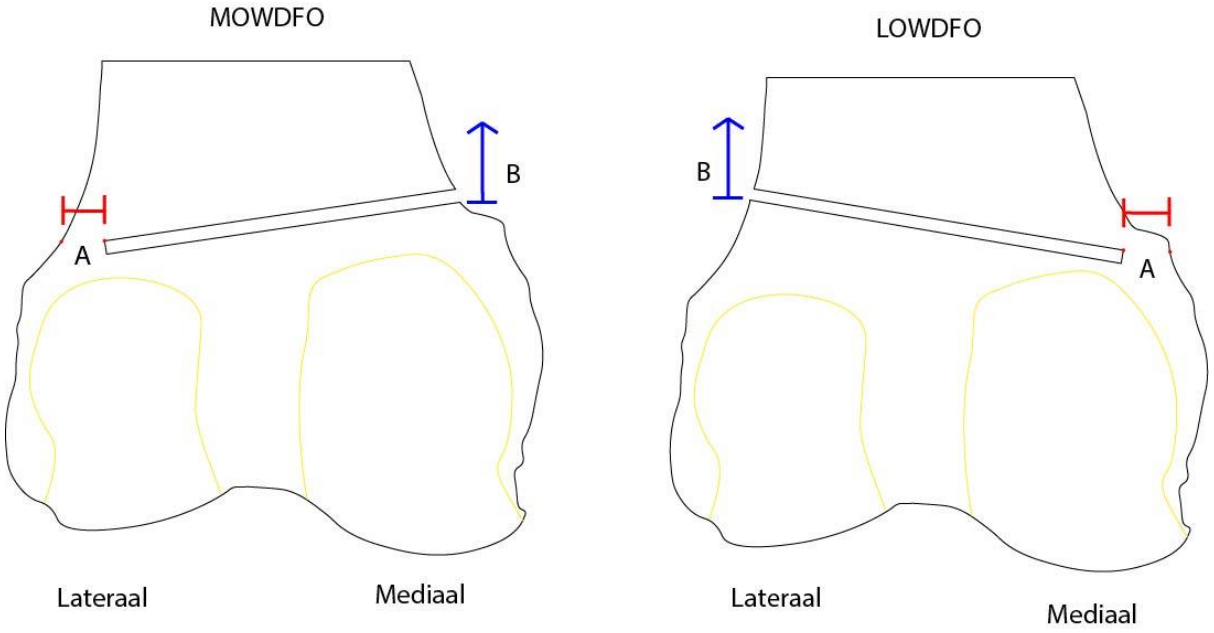

Figure 9. The variables for both the medial open wedge DFO(left) and lateral open wedge DFO(right). Where A is the hinge size and angle of the osteotomy plane is B. These variables can be changed creating multiple models.

Angle of the osteotomy plane

The angle of the osteotomy plane is defined as the angle between the transverse plane that touches both condyles and the plane of the osteotomy saw. This angle is influenced by the hinge location, hinge size, and the location of the saw insertion. However, the optimal angle has not been thoroughly researched in the literature. The lowest point is determined as the most distal point where a saw incision could be made without damaging the cartilage. To vary the angle without altering the hinge location and size, the starting point of the saw cut must be adjusted.

In collaboration with orthopedic surgeons from UMC Utrecht, it was decided to use increments of 2.5 mm, as this approximates the precision achievable during surgery. For this research, heights of 0, 2.5, 5, 7.5, and 10 mm were chosen. To create these models, the plane created from the incision point is offset by the predefined amounts. This results in five different models where only the angle of the osteotomy gap differs.

Model including drill holes

To assess the impact of drill holes on hinge fractures, two models were created: one with drill holes and one without. The drill holes were introduced after the creation of the osteotomy plane in state 1. Additionally, the unaltered model was generated following the previously described process.

For the model with drill holes, modifications were made to state 1. The drill holes were added after establishing the osteotomy plane. Two drill holes were inserted to intersect the osteotomy plane, as depicted in Figure 11. The midpoint of each drill hole was aimed towards the proximal corner of the osteotomy plane to round off that corner. The entry point for each drill hole was strategically selected to be accessible from the front of the osteotomy gap, ensuring ease of access during the osteotomy procedure.

State 2 was not simulated for this model, as the primary objective was to compare it with other research where only state 1 was modelled.

Unaltered model

The unaltered model was created by importing a femur without an osteotomy gap and implementing the steps described in state 2, excluding the use of a plate. In this model, the distal femur was fixed at the condyles, and loading was applied to the femoral head, following the procedure outlined in Chapter 2.6. The purpose of this model is to serve as a baseline for comparison with the modified models that incorporate osteotomy gaps and plates.

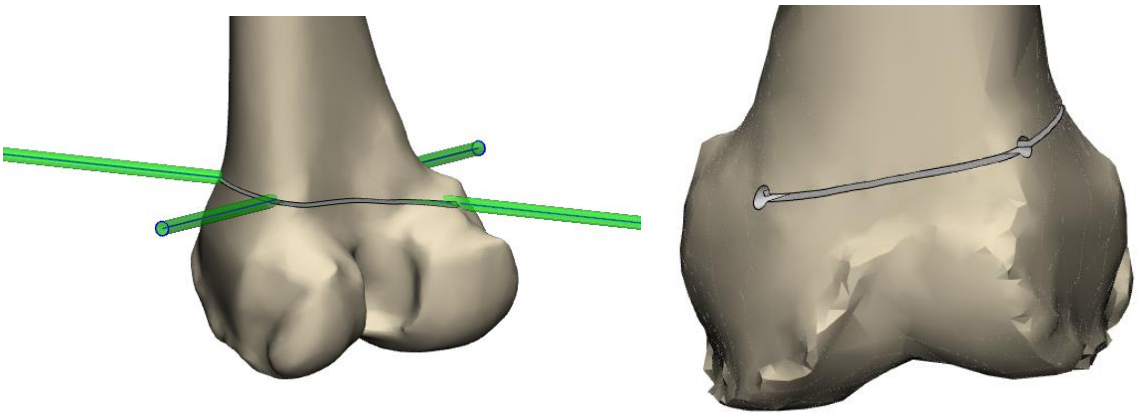

Figure 10. A visualisation of the drill holes on a lateral open wedge DFO. As can be seen the drill holes are directed toward the distal corner of the osteotomy gap before the gap is opened.

Additional model with screws

To explore the impact of plate location and screws, an additional model was created to investigate these differences. This was achieved by re-importing the deformed model from state 1 into 3-matic and using the plate placement as a reference. The screws were replaced by cylinders with a diameter of 4.5 mm. The material of the femur occupied by these screws was subtracted from the femur. This process is illustrated in Figure 11. This model provides insight into how the plate is positioned on the femur for both medial and lateral open wedge DFO procedures.

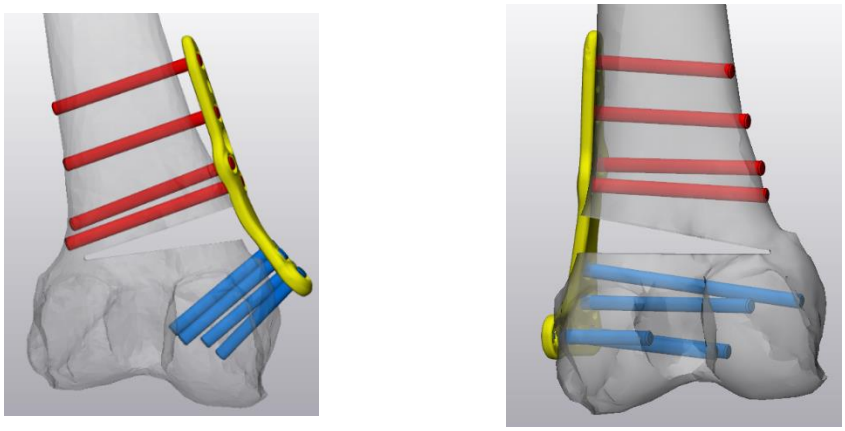

Figure 11. Left the medial open wedge DFO right the lateral open wedge DFO both including screws

The material of the screws is defined as Ti-64, the same as the plate. The femur is considered uniform because, due to technical limitations, the material properties from state 1 could not be copied. The Young's modulus of the femur was chosen to be 14 GPa [38]. This was mainly selected because the main interest lies in the cortex. The connection between the plate and screws can be considered rigid due to the use of locking screws and was simulated as such. The surfaces of the femur and screws are tied together, replacing the previous connection between the femur and the plate.

2.8. Automatization of the creation of the FEM models

In this subchapter, the automation of the process is discussed, as illustrated in Figure 12. Automating the model generation process provides the ability to produce multiple models with specific changes that can then be compared. This ensures that only defined variables, such as hinge size and angle of the osteotomy plane, among others, are different, while the rest of the model remains consistent. This approach minimizes human error and bias while also eliminating repetitive work.

A combination of 3-matic, Mimics, and Abaqus was utilized to automate the creation of these models. All programs offer both a visual interface and can be controlled using a Python interface. Only the creation of the lateral open wedge DFO model will be discussed, as most alterations are minor compared to this model.

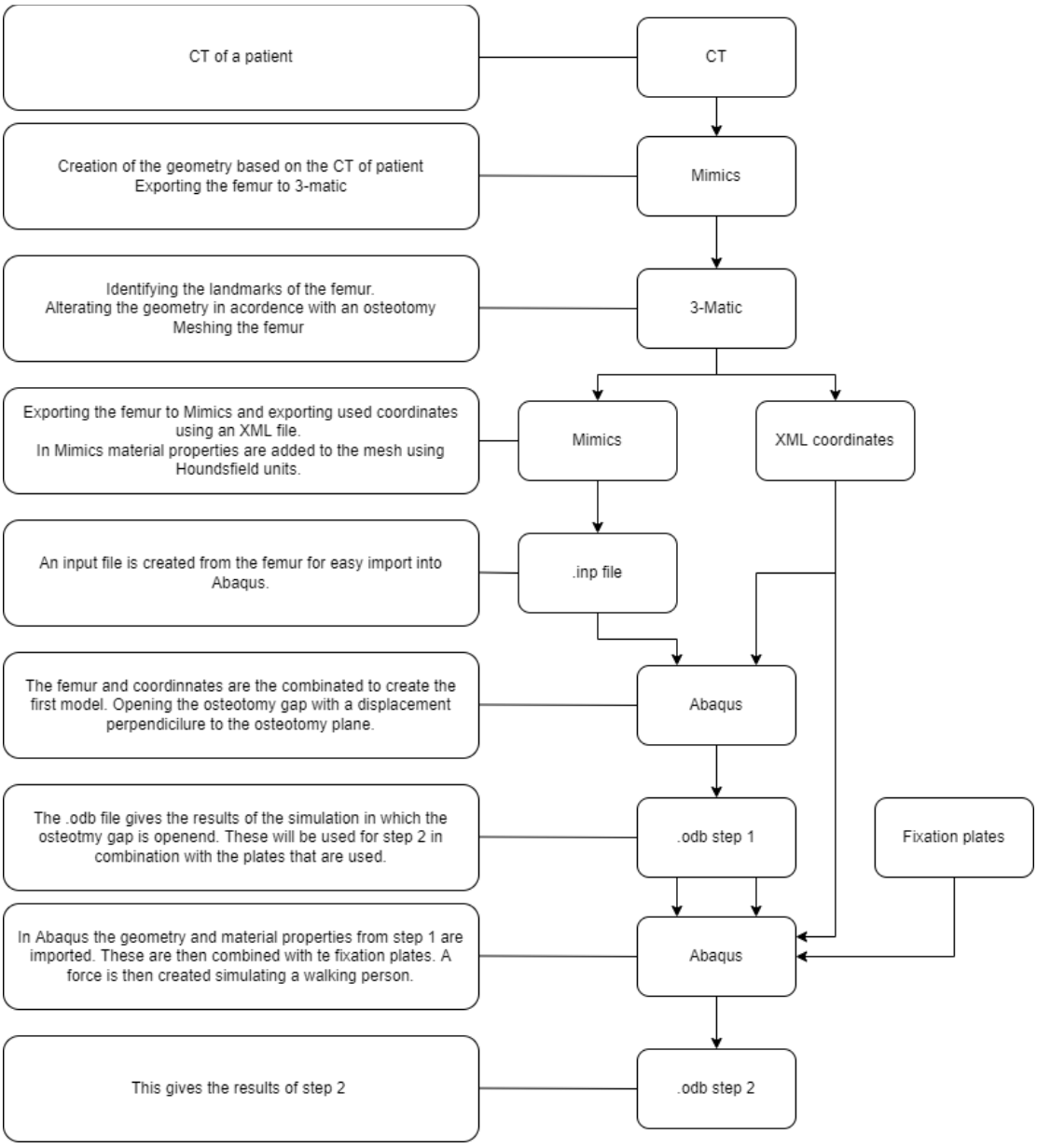

Figure 10. A flowchart showing the creation and automation of the model creation

For automation, a file structure was required to store temporary files. This structure is depicted in Figure 13. Each process has its individual folder to store files, thus preventing naming conflicts. Moreover, old files can be preserved, enabling a process to be repeated if necessary.

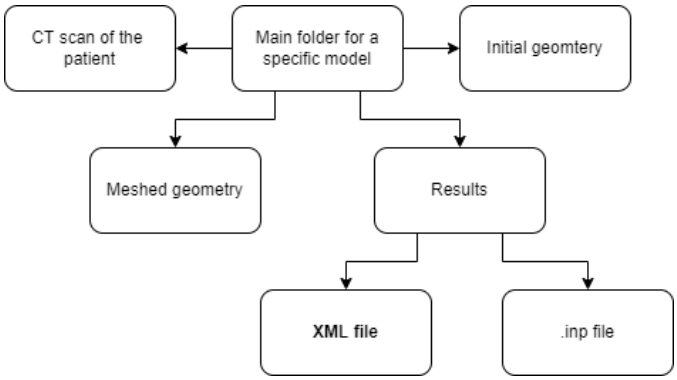

Figure 11. The folder structure used for the automation of 3-matic and mimics

The initial step is not automated, as it involves creating the initial geometry of the femur from a CT scan. This step is not automated because the initial model will be reused each time and was only created once. The model obtained from this step remains unchanged in the folders and can always be found in the "initial geometry" folder.

Subsequently, the initial geometry is imported into 3-matic, where in-house developed automated software is used to automatically select the landmarks of the femur. The main landmarks include the center of the femoral head, the mechanical axis, the planes of the femur, and the location of the condyles.

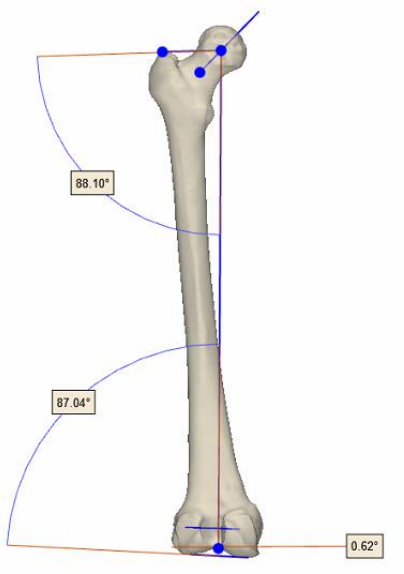

Figure 12. Here some landmarks are shown

These landmarks are then utilized to create the osteotomy gap. The process involves defining the starting point of the saw cut and the location of the hinge. This is carried out from the sagittal plane of the femur since the osteotomy gap is created from this direction. By adopting this approach, the creation of the 3D osteotomy gap can be initiated by generating a 2D line on the sagittal plane. Both the hinge location and the point where the saw enters the bone must be manually determined, allowing orthopedic surgeons to select their preferred locations on an individual femur.

These points are then translated into planes offset from the transverse plane of the femur. The most lateral location of the femur is chosen for the incision into the bone, while the most medial location is identified for the hinge location. An offset of 10 mm from the most medial location is used to create the hinge. With these two points and the sagittal plane, the osteotomy gap is formed. This is achieved by creating a plane perpendicular to the sagittal plane of the femur, with its midpoint at the incision location and extending to the hinge location. The plane is then extruded by 1.2 mm, corresponding to the size of the oscillating saw used during osteotomies. In cases of different hinge sizes or osteotomy plane angles, an offset is applied to create the alternative sizes or angles. If multiple hinge sizes and angles are selected, multiple models will be generated.

Once this step is completed, the geometry is finalized and the model can be meshed. Since the focus is on the hinge area, a finer mesh is applied around the hinge. The coordinates are determined based on the hinge location, with "x" above the hinge, "y" below, and "f" in front until reaching the cortex of the femur. The proximal corner of the osteotomy gap is considered as the hinge location.

When transferring files from Mimics to Abaqus, only the models can be sent, as points and lines cannot be exported due to limitations of the file formats used. However, since these elements are essential for creating sets and boundary conditions, they need to be transferred differently. To address this, 3-matic exports an XML file that can be later imported into Abaqus. This file can be directly imported into Mimics as well.

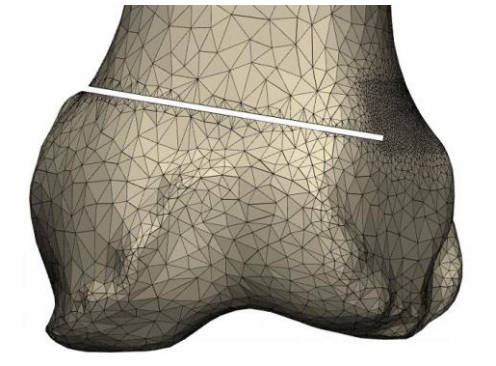

Figure 13. Here a mesh is shown. A higher density of elements can be observed around the hinge

The subsequent step involves adding material properties to the femur. To accomplish this, we import the 3-matic file into Mimics. The original CT file is imported and utilized to assign densities based on Hounsfield units. These assigned densities can then be employed to calculate a Young's modulus using the formulas discussed in Chapter 2.6. Following this, the model is exported to Abaqus using the .inp file extension.

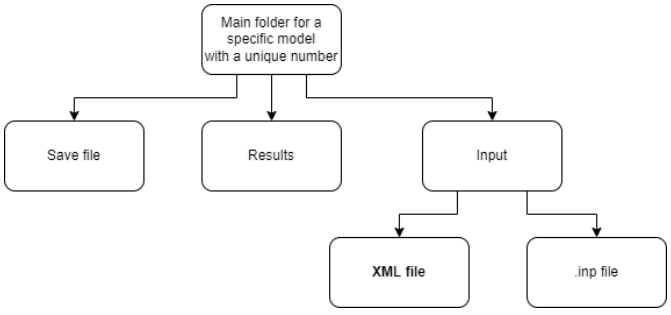

Figure 14. The folder structure used to automate Abaqus

This model can then be utilized in Abaqus to create state 1. A simulated wedge is inserted into the saw opening, using locations imported from earlier steps. This can be observed in Figure 17, where the end result is visible.

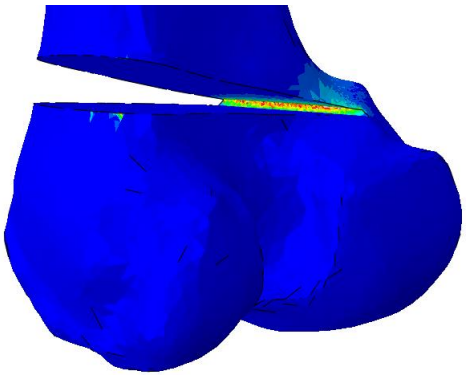

Figure 15. An example where the osteotomy gap is shown here were a simulated wedge is used to open the gap

State 2 continues with the geometry created after completing state 1. The plate has to be added manually, along with the connection points linking the plate and femur, among other elements. For example, refer to Figure 18. Additionally, in Figure 19, a real-life example is provided for comparison.

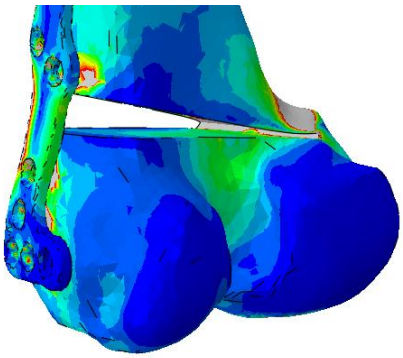

Figure 16. An example of the model where the plate is virtually attached to the femur

Figure 17. An in vivo example

3. Results

In this chapter, we will examine the results obtained from the simulation of the models described in the materials and methods section. This was conducted model by model, providing an overview of the results for each model.

3.1. Medial open wedge DFO vs Lateral open wedge DFO

Models were created for both the medial and lateral open wedge DFO. This process occurred in two steps. The first step, referred to as state 1, involved opening the osteotomy gap. The second model, referred to as state 2, simulates the forces experienced when the patient resumes walking.

State 1:

As depicted in Figure 20 and Figure 21, the differences at state 1 are minor. There is a slightly higher strain observed in the medial open wedge DFO compared to the lateral, although the difference is not significant. In both cases, the highest stress and strain concentrations were observed in the frontal proximal corner of the osteotomy gap.

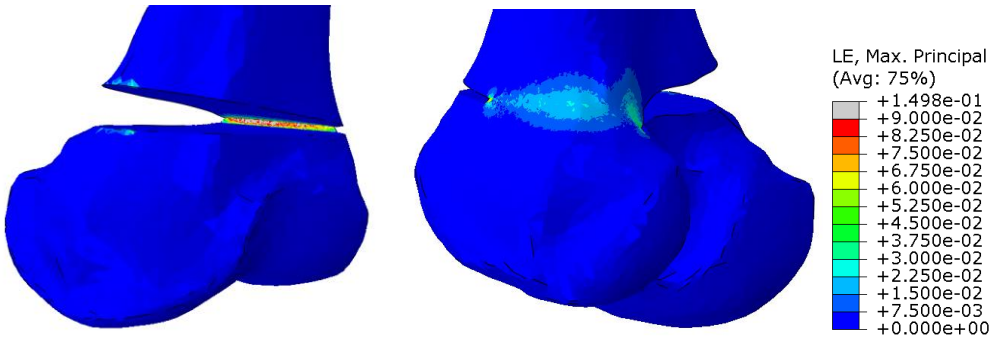

Figure 18. Medial open wedge DFO opening of the osteotomy gap

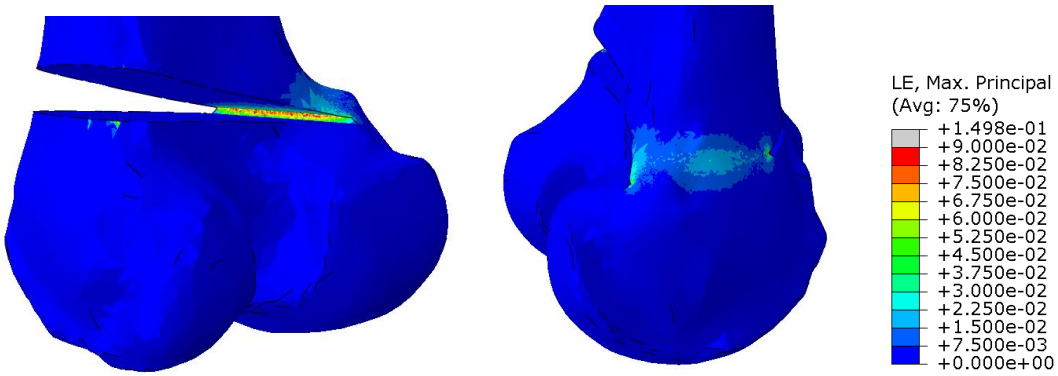

Figure 19. Lateral open wedge DFO opening of the osteotomy gap

State 2:

In state 2, where the forces of a gait are simulated on the femur, the initial assumption was that the hinge of the medial open wedge DFO would be under tension due to the difference in the anatomical and mechanical axis in the femur, as depicted in Figure 19 and 20. However, no tension was observed in either the hinge of the medial open wedge DFO or the lateral open wedge DFO. This indicates that the initial assumption was not supported by the experiment, and other explanations should be explored for the difference in hinge fractures between medial and lateral osteotomies.

When comparing the medial open wedge DFO and lateral open wedge DFO models, a significant difference can be observed. As illustrated in Figure 22 and Figure 23, the hinge of the lateral open wedge DFO experiences significantly more strain and stress than the medial open wedge DFO. This difference can be partially explained by the force distribution between the medial and lateral compartments of the tibiofemoral joint. Approximately 60% of the force applied to the head is distributed to the medial compartment and 40% to the lateral compartment, which may contribute to the observed difference[2].

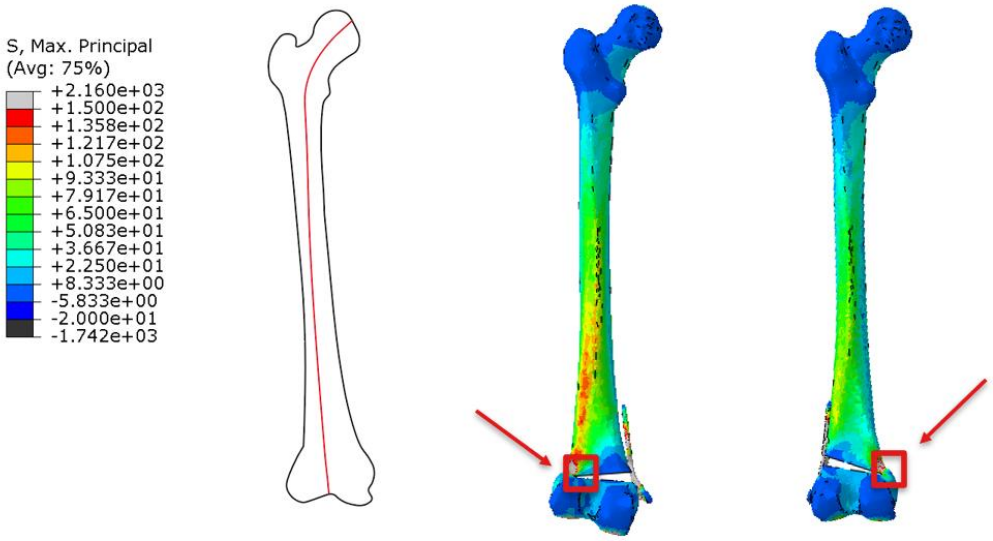

Figure 20. From left to right curvature of the femur followed by the medial open wedge DFO and lateral open wedge DFO. The red squares are pointed toward the hinge of both hinges.

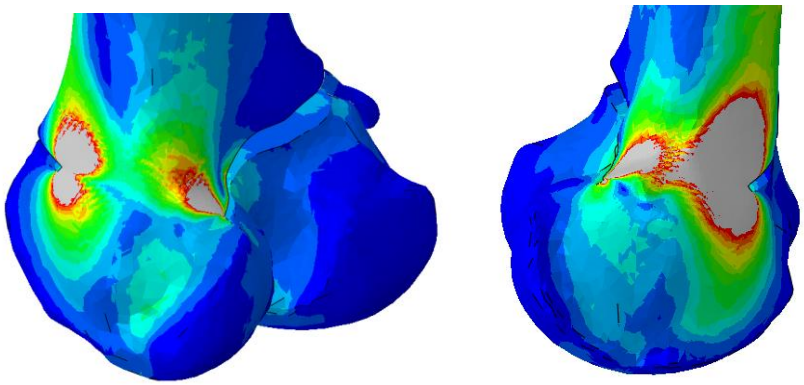

Figure 21. Medial open wedge DFO on the left lateral open wedge DFO on the right zoomed in from the previous figure

3.2. Hinge size

In this experiment, five different hinge sizes were investigated: 5 mm, 7.5 mm, 10 mm, 12.5 mm, and 15 mm. These various hinge sizes will be compared for both the model simulating the opening of the osteotomy gap (state 1) and the model simulating a walking person (state 2).

State 1:

All five sizes were opened to 10 mm since the process is based on displacement, the force to open each osteotomy gap differs. A relationship between the size of the hinge and the force necessary to open it was observed. As shown in Figure 24, a larger hinge required significantly more force to open. The additional material that has to deform in larger hinges can account for the larger amount of energy necessary to open the hinge.

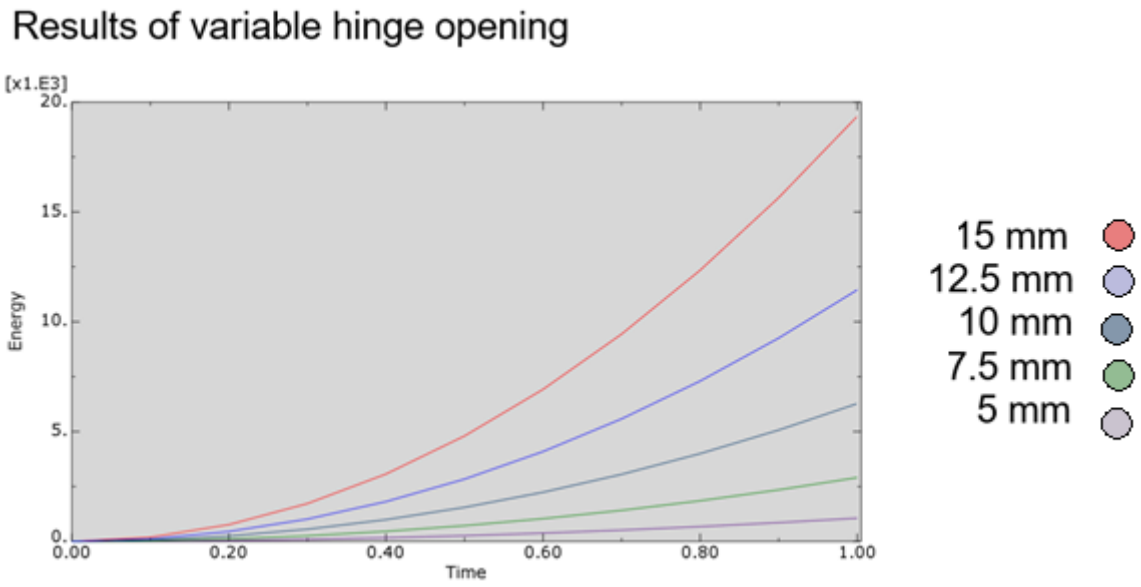

Figure 22. Showing he different amounts of energy required to open osteotomy gaps with different sizes.

The hinge size also influences the hinge location. This hinge point is closer to the osteotomy gap than the medial cortex. This can be observed if a line is drawn from the highest strain area in the top corner of the osteotomy gap through the high strain areas to the medial cortex, as can be seen in Figure 25.

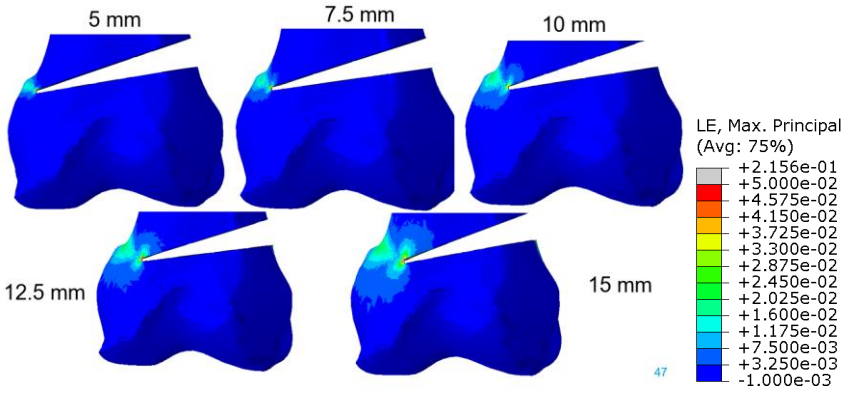

Figure 23. showing the strain of five different models with different hinge sizes.

State 2:

In state 2, a force is applied to the 5 models. The differences can be seen in Figure 26. In the 5 mm hinge, a significant increase in strain can be observed, which also translates to low rotational stiffness.

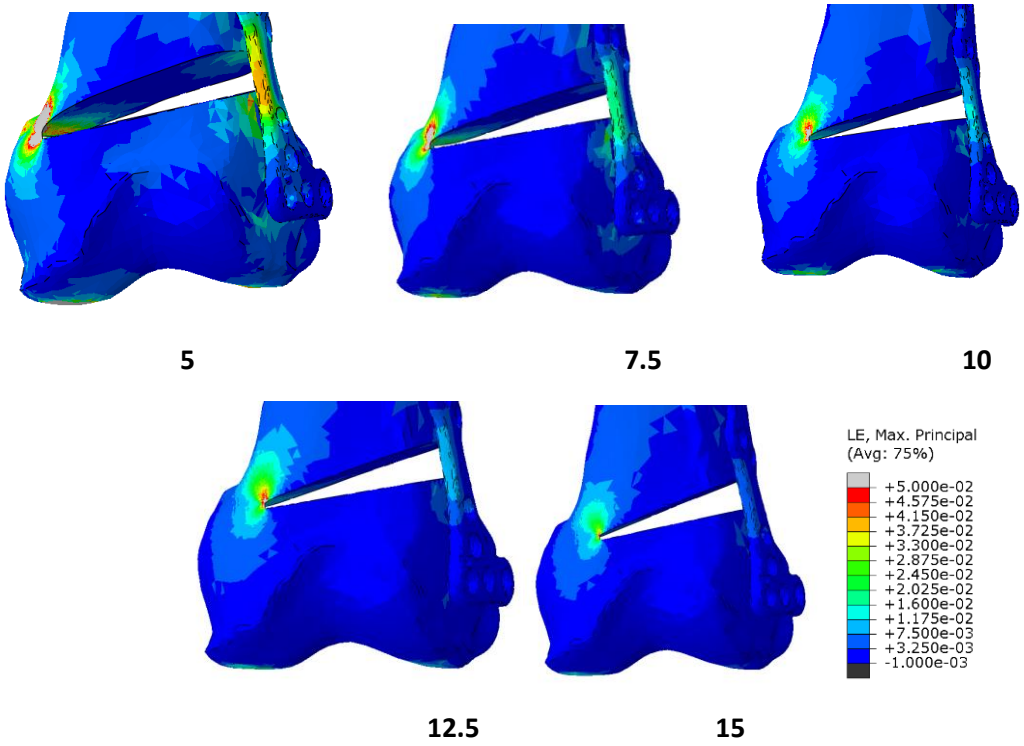

Figure 24. Moment 2 a femur during gait. From left top to bottom right 5 mm, 7.5 mm, 10 mm, 12.5 mm and 15 mm

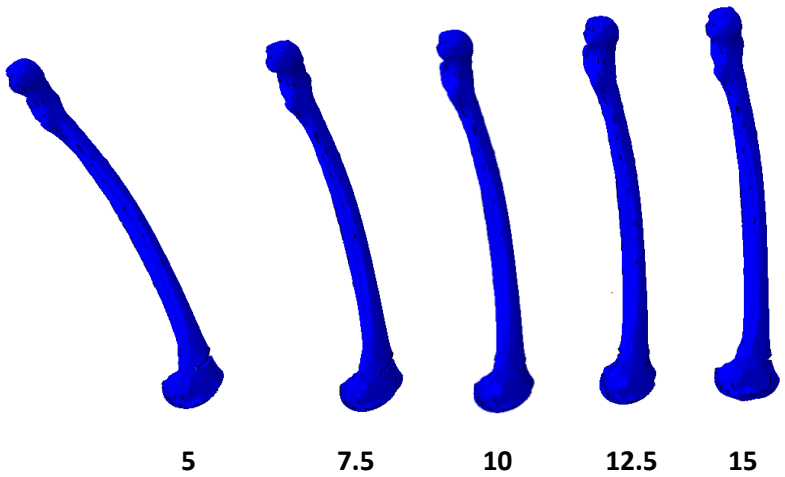

Figure 25. Lateral open wedge DFO with different hinge sizes from left to right 5, 7.5, 10, 12.5 and 15 mm. Showing the displacement.

As observed in Figure 26 and Figure 27, both the 5 mm and 7.5 mm hinges deform significantly when loaded. Larger hinges seem to provide more stiffness against rotational movement. However, at both 5 mm and 7.5 mm, a significant displacement can be observed (as shown in Figure 12), which is so great that the material would fail[41].

Osteotomy Angle: Using a different height for the incision in the femur changes the osteotomy angle, resulting in multiple models. The effect of this angle has not been researched in previous finite element studies.

This was achieved by choosing different incision heights of 0 mm, 2.5 mm, 5 mm, 7.5 mm, and 10 mm, as shown in Figure 10. The results of these models can be seen in Figure 28..

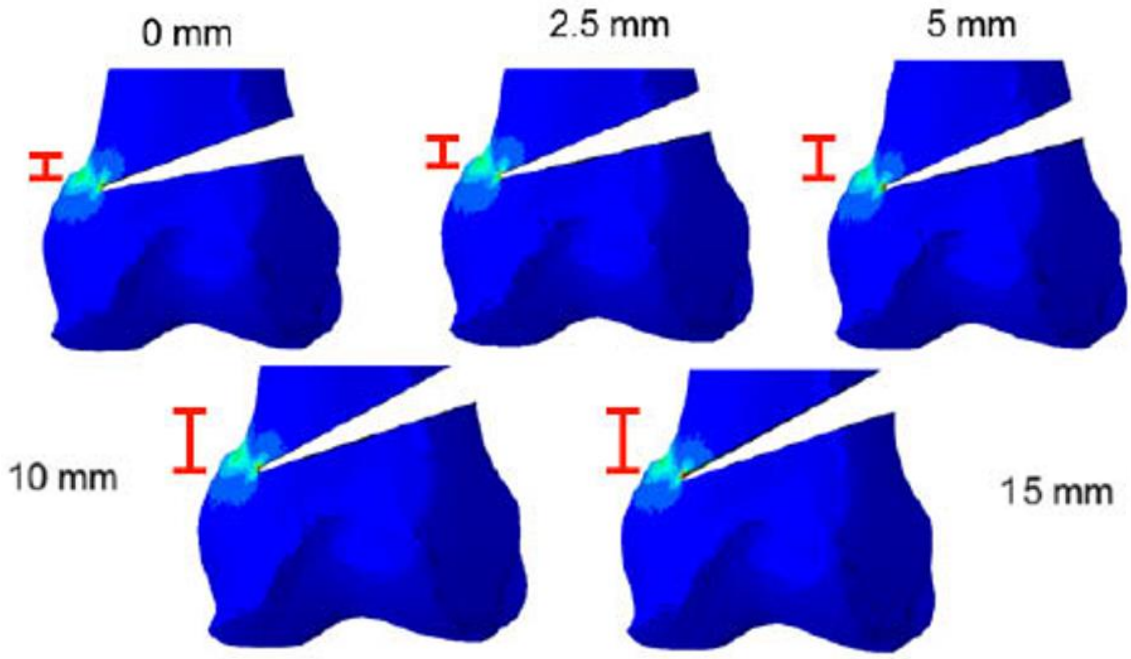

Figure 26. The five different models from left top to right bottom 0, 2.5, 5-, 7.5- and 10-mm higher incisions changing the angle of the osteotomy gap

No significant differences can be observed between the different models. A small change can be observed in the proximal frontal corner of the osteotomy gap. In the higher osteotomy angles, an increase in the stress concentration around the proximal frontal corner of the osteotomy gap can be observed.

3.3. Drill holes

Comparing drill holes to the regular situation, these drill holes are different from the ones proposed in current literature and could be created in a less invasive way while possibly achieving the same results.

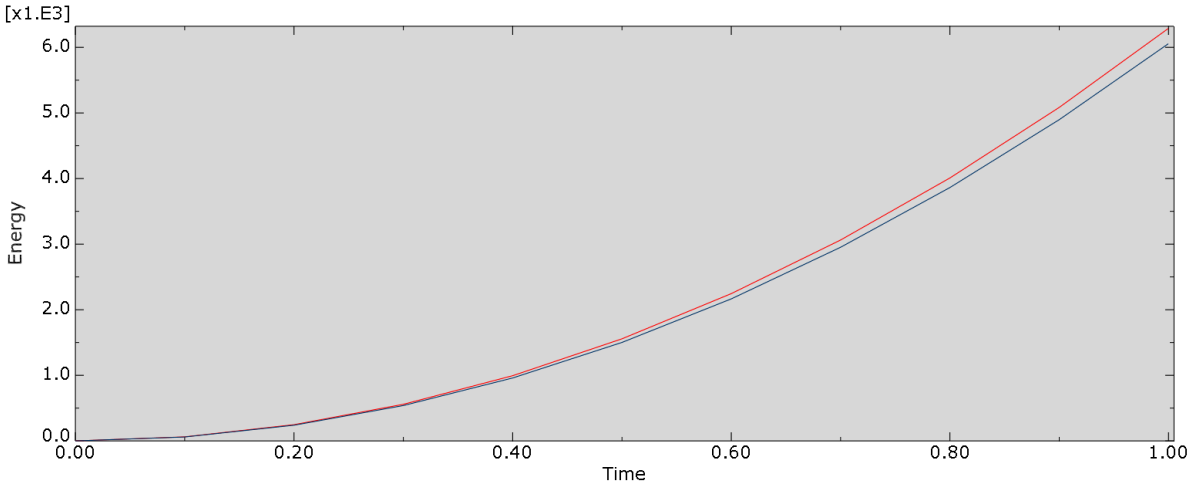

Figure 27. The amount of energy required to open the osteotomy gap red is without drill holes.

As can be seen the removal of material leads to a decrease in energy that is required to open the osteotomy gap to 10 mm. This is to be expected since less material must be deformed.

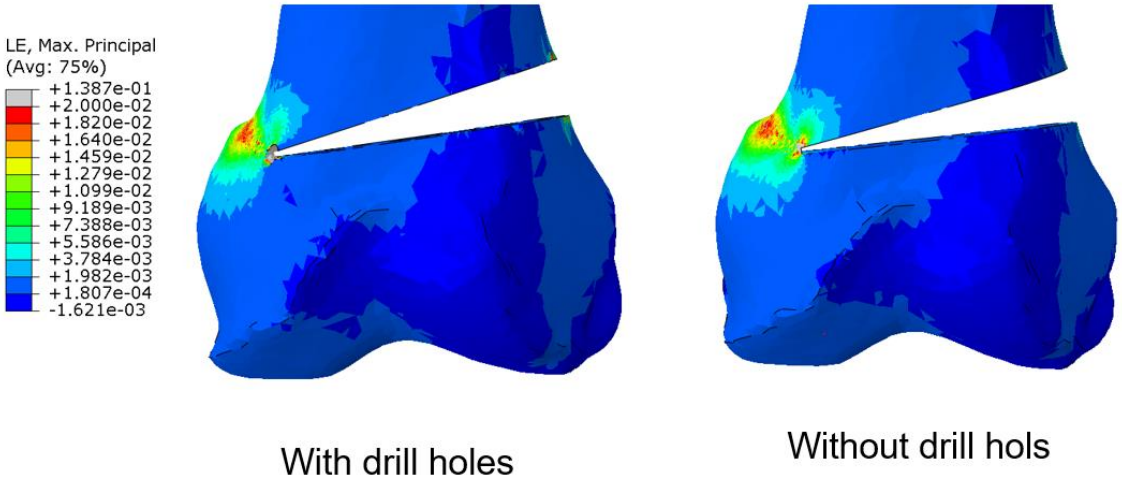

Figure 28. The strain of two models one with and one without drill holes in the corners is shown

Since the material that is removed by the drill holes would be under the highest amount of strain, it is expected to extend the size of the osteotomy gap that can be opened without initiating a fracture. Furthermore, it moves the highest strain and stress point away from the corners. However, it has the disadvantage that less material is available when the femur receives a load.

3.4. Model with screws

An important distinction between the medial open wedge DFO and lateral open wedge DFO is the plate used. Since there was no specifically designed plate available for the medial open wedge DFO, a lateral closed wedge DFO plate was used from the contralateral side.

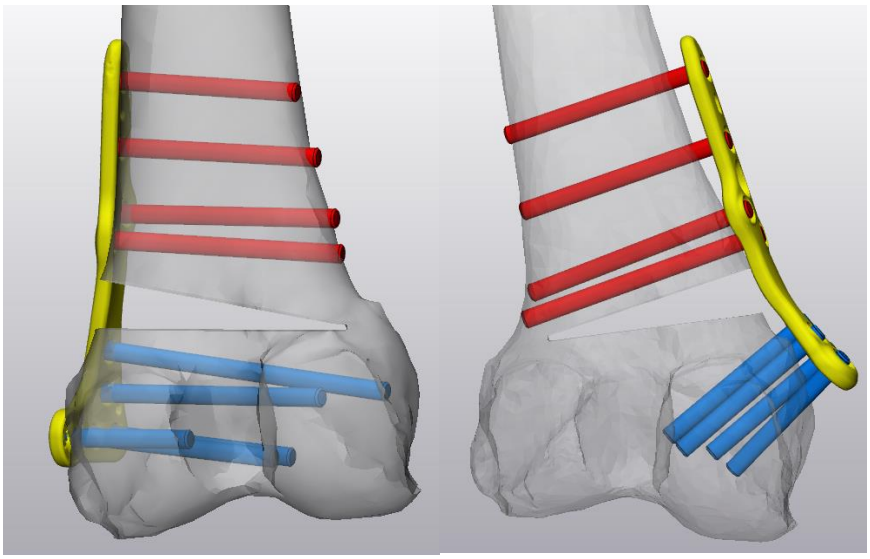

Figure 29. This figure shows the plates and screw placement of both the medial open wedge DFO (left) and lateral open wedge DFO(right)

In Figure 31, the locations of the plates can be seen as created in the model. The placement of the plates was based on radiograph pictures and discussions with doctors. As observed in the MOWDFO, the screws are closer to the hinge. It is uncertain if this difference always occurs, possibly due to the absence of a specialized plate for the MOWDFO.

Figure 30. Two examples of the plate and screw location of medial open wedge DFO with fractured hinges.

The created finite element models reveal that the stress concentrations around the most distal screws of the proximal part of the plate coincide with the stress concentration around the hinge in the medial open wedge DFO. However, this is not observed in the lateral open wedge DFO model due to the larger distance between the screws and the hinge. The interlocking stress and strain fields of the medial open wedge DFO can be seen in Figure 34, whereas this phenomenon is absent in the lateral open wedge DFO model shown in Figure 33. In the medial open wedge DFO model, the screws appear to weaken the cortex, leading to greater tension concentrations around them.

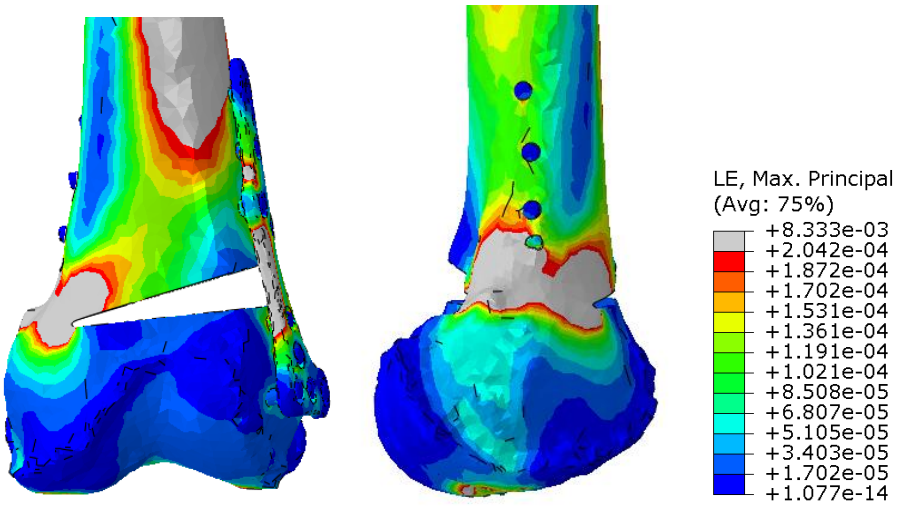

Figure 31. Lateral open wedge DFO model 2

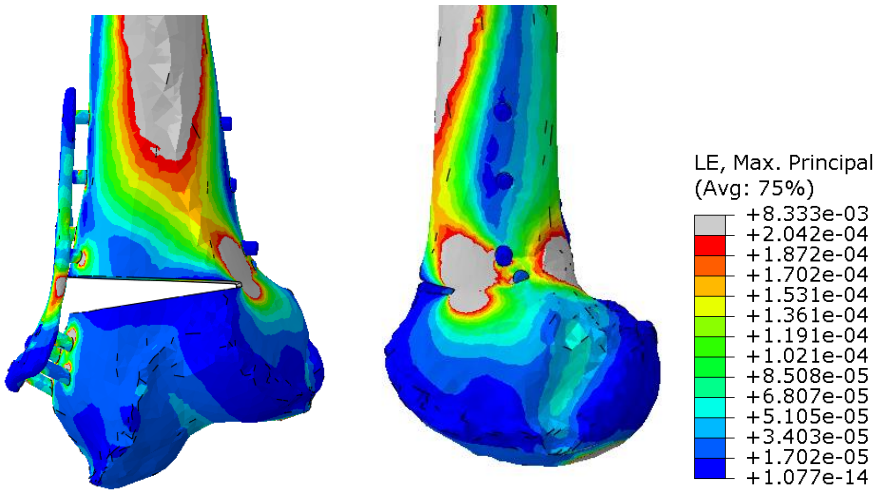

Figure 32. Medial open wedge DFO model 2

4. Discussion

In total, seven different types of finite element models were utilized to analyse various aspects of osteotomies. Each model underwent a detailed analysis focusing on its specific attributes as well as any shortcomings identified during the study.

4.1. Model validation, mesh dependency and unaltered model

The unaltered model underwent rigorous testing for mesh convergence and was compared to similar finite element models from the literature, as described in section 3.1. The mesh was thoroughly checked for possible errors, and none were found in the models used. Mesh convergence was observed, but a smaller element size was chosen to account for the partial volume effect of the Hounsfield units.

Furthermore, the models were validated by comparing them to earlier created finite element models of femurs in simulated gait, as depicted in Figure 13. The combination of both mesh convergence and similarity to other models provides an indication that the model is accurate.

To further validate the model against existing literature, the unaltered model was utilized. This decision was made because no lateral open wedge DFO finite element models could be found in the literature. Papers were selected based on the use of simulated gait in the created models. Some papers demonstrated similar stress and strain distribution, further bolstering the credibility of the model [39][40].

4.2. Medial open wedge DFO vs Lateral open wedge DFO

It was discovered that the medial open wedge DFO model does not subject the hinge to tension, thus leading to the dismissal of the initial hypothesis in this specific scenario. However, this leaves the question of the increased occurrence of hinge fractures unanswered. Upon examination of the differences in state 1, they are relatively minor, with slightly higher strain and stress observed in the medial open wedge DFO.

In contrast, the differences become more pronounced in state 2. The lateral open wedge DFO exhibits significantly more deformation and stress compared to the medial open wedge DFO. This discrepancy can be partially attributed to the distribution of forces between the medial and lateral sides of the femur. The unaltered model serves as an illustrative example, demonstrating that the medial side of the femur bears more force. This observation is consistent with findings from other studies, which have also reported a similar force distribution between the lateral and medial femur/knee joint. Such findings may offer insights into the underlying reasons for the higher incidence of hinge fractures.

The increased occurrence of hinge fractures (HF) in medial closed wedge DFO compared to lateral open wedge DFO presents an intriguing phenomenon, [42] particularly considering that closed wedge osteotomies typically have lower rates of hinge fractures. One potential explanation for this discrepancy could be differences in the material properties of the hinge between medial open wedge DFO and lateral open wedge DFO.

The unaltered model demonstrates that during a normal gait, the stress and strain on the medial side of the femur are significantly higher. This observation, based on a single loading condition, suggests that the lateral side, where the hinge of the medial open wedge DFO is located, may be less resistant to strain. This assumption is predicated on the notion that bone exhibits adaptive, anisotropic

properties. Further research into these material differences could shed light on the underlying causes of the disparity in hinge fractures.

Understanding the precise moment at which hinge fractures occur would be crucial in devising preventive measures. For instance, if fractures predominantly occur during state 1, reducing the hinge size might be beneficial, whereas if fractures occur during state 2, enlarging the hinge could be considered. This avenue of investigation could be explored in a follow-up study focusing specifically on the occurrence of hinge fractures, possibly by analysing a large dataset where the exact moment of fractures is documented.

The choice of plate used may also contribute to the occurrence of hinge fractures. In the model of lateral open wedge DFO including screws, an overlap of stress concentration zones is observed (Figure 33). This overlap could potentially compromise the hinge, particularly as it coincides with the location where a type 2 hinge fracture would be expected. Moreover, the smaller surface area of the medial open wedge DFO hinge may exacerbate stress concentrations, especially if an initial fracture compromises the hinge.

Overall, the reasons for the difference in hinge fractures between medial open wedge DFO and lateral open wedge DFO remain poorly understood. As such, no conclusive steps can currently be taken to prevent hinge fractures in medial open wedge DFO. Further research in this area is warranted to elucidate the underlying mechanisms and develop effective preventive measures.

4.3. Hinge size

The ideal hinge size in current literature is predominantly cited as 10 mm, although substantial evidence supporting this assertion appears to be lacking. This thesis aims to investigate the optimal hinge size using multiple models.

The ideal hinge size in current literature is predominantly cited as 10 mm, although substantial evidence supporting this assertion appears to be lacking. This thesis aims to investigate the optimal hinge size using multiple models.

For the opening model (state 1), a hinge size as small as possible appears most favourable, as it results in the lowest stress and strain. Previous research has indicated that hinge sizes larger than 10 mm are prone to hinge fractures (HF) during the opening of the osteotomy gap

[26][45] , particularly creating unstable hinge fractures. The findings of this study support these assertions, demonstrating significant energy for potential fractures and high stress and strain concentrations at larger hinges. Therefore, hinge sizes of 10 mm and smaller are deemed ideal for state 1, a conclusion reaffirmed by the results of this study.

In contrast, when considering state 2, the models created suggest that hinge sizes of 5 mm and 7.5 mm result in significantly unstable hinges. During simulated walking, these hinge sizes compromise rotational stiffness and present a high risk of damage. This leaves hinge sizes of 10 mm, 12.5 mm, and 15 mm as the most viable options for state 2, with larger hinges appearing more beneficial.

It is worth noting that previous research has indicated that hinge sizes larger than 10 mm are prone to hinge fractures, specifically those that are unstable. While the models of 5 mm and 7.5 mm hinges demonstrate insufficient strength, pointing to the 10 mm hinge as the preferred size based on the assumptions made in this research.

It is plausible that variations in bone material properties due to factors such as age, sex, genetics, activity level, and potential diseases could influence the ideal hinge size, as fractures may occur with

less stress or strain. The method and automation developed in this thesis offer a means to investigate this by employing various femurs with assigned different material properties[46]. However, achieving precise hinge sizes during surgery may pose challenges, suggesting that while an ideal hinge size can be theorized, practical application may vary for each individual subject.

4.4. Osteotomy gap angle

While the angle of the osteotomy gap appears to have a slight impact on the stress concentration at the proximal frontal corner of the osteotomy plane, the effect is minimal. The optimization resulting from adjusting the osteotomy angle would likely be so negligible that it would not justify the associated costs.

This finding aligns with current surgical practices, where the location of the incision in the bone is typically kept as low as possible. Furthermore, the design of plates currently in use often dictates this location, further supporting the notion that the potential benefits of optimizing the osteotomy angle may not outweigh the practical considerations and costs involved.

4.5. Drill holes

Using drill holes across the osteotomy plane, as tested in this thesis, primarily removes material that is under the most strain. However, the remaining material continues to experience the same level of strain. While this method may offer a more practical approach to reducing stress around the hinge compared to current techniques, as it is less invasive and does not require additional access locations, there are challenges to consider.

One significant challenge is the precision required. Accurate identification of the exact location of the corners of the osteotomy gap and precise aiming for these locations are essential. While patient-specific instrumentation could enhance precision, achieving the necessary level of accuracy may be challenging. Inaccurate drill hole placement could result in significant complications, potentially causing harm to vital tissues.

While drill holes appear effective in relieving stress concentrations and transferring strain from the cortex to trabecular bone, which can withstand higher strain rates, they may not be sufficient to prevent all fractures, particularly in cases of very brittle bones or large corrections. Additionally, some studies suggest that drill holes could actually lead to increased stress concentrations. Furthermore, removing material from the hinge may result in less material carrying a higher load, potentially compromising structural integrity.

4.6. Open points

Due to time limitations and technical constraints, several paths of research were considered but not fully explored in this study. Initially, changes in hinge size and angle of the osteotomy gap were incorporated into the models. Additionally, other variables such as altering material properties to simulate different ages and possible diseased states, transversal rotation, and the size of the correction were also contemplated but not thoroughly investigated.

Since the initial hypothesis was rejected and no tension was found in the medial open wedge DFO, alternative causes needed to be considered. Fracture mechanics was one such consideration, leading to an investigation of options available in Abaqus, including J and Ct integrals. However, a limitation arose due to the restricted choice of elements in 3-matic and Mimics, which only allow for the use of tetrahedral elements, rendering J and Ct integrals unusable. Another concept explored was XFEM, which offers fracture modelling based on non-mesh-dependent mechanics. Although XFEM showed

promise, its reliance on significant computing power posed limitations, especially when considering bone as a more uniform material.

Ultimately, these options were not implemented due to the need for creating entirely new models, which was not feasible within the given time constraints. Additionally, certain aspects such as fracture mechanics required specialized knowledge that was not readily available.

4.7. Automation

A significant portion of the process was automated in this study. However, since only one femur was considered, no comparisons could be made between different patients. In more complex cases, such comparisons could offer valuable insights into individual patient geometries. Some limitations were encountered in the automation process due to the choice of software, but these were largely manageable with adjustments to the setup. For instance, having Abaqus, 3-matic, and Mimics on different computers led to file transfer issues, highlighting the potential benefits of having all software on a single system.

Further refinement and automation of this process could provide insights into cases involving low bone density or other conditions, especially when compared across multiple cases. This could offer valuable insights into factors contributing to hinge fractures based on different model parameters. The automation demonstrated in this thesis suggests that it is feasible to automate significant portions of the process.

However, challenges remain, particularly in Abaqus. One main challenge is the selection of regions, as Abaqus lacks robust tools compared to 3-matic and Mimics. One workaround involves importing landmarks via the XML file and using coordinates created in 3-matic.

Overall, the automation efforts were successful in reducing model creation time and increasing accuracy through the replication of multiple models. However, the accuracy and clinical utility of these models are still limited due to the complex nature of bone, loading conditions, and the current understanding of non-linear problems like fracture mechanics. Achieving greater precision in these models would require expertise from multiple fields, including orthopedics, engineering, and mathematics[47].

4.8. Limitations

The use of Hounsfield units to determine bone density has several limitations. While it has been demonstrated that bone material properties are partially dependent on density, with approximately 43-72% of the properties explained by density, [48] bone is actually an anisotropic material. However, in this study, bone was considered isotropic, which may introduce inaccuracies compared to real-world conditions. Additionally, the CT scans used in this study were not consistent with those used in previous studies that established the parameters based on Hounsfield units. The differences in CT scan settings and techniques could further contribute to inaccuracies in the determination of bone density[30].

Furthermore, both the CT scan and the use of Hounsfield units are susceptible to the partial volume effect, particularly in areas where the cortical bone is thin, such as around the hinge area. This effect can lead to lower density values being measured due to the inclusion of surrounding lower-density tissues in the calculation [50]. Moreover, when assigning material properties to finite elements, the density is averaged over the entire element, introducing another aspect of the partial volume effect.

Overall, while the use of Hounsfield units provides a method for estimating bone density, it is important to recognize the limitations and potential inaccuracies associated with this approach, particularly in areas of thin cortical bone and when considering the anisotropic nature of bone. Further refinement of techniques and consideration of these limitations may improve the accuracy of finite element models in predicting bone behaviour.

The different models in this study continue using the geometry from the previous step, but without carrying over the stress from the previous step. This decision was made to simplify the creation of the models, but it can lead to issues where stress concentrations created in successive steps may not be accurately represented. To address this in future models, copying stored variables corresponding to node numbers could be implemented since they remain constant.

In this study, a healthy femur was used for all models to perform both medial open wedge DFO and lateral wedge DFO. While using the same femur allowed for comparison of the studied variables, it may result in non-realistic results as the chosen femur did not have deformities such as valgus or varus, which many patients undergoing osteotomy have. Varus and valgus deformities could lead to differences in material properties and force distribution throughout the femur. Although these differences might not be extreme, it would be valuable to compare them with a healthy femur. Additionally, the femur chosen was based on availability rather than quality.

In the main model used, screws are not incorporated, and the interaction is solely between the plate and femur. While this simplification aids in calculations, it also compromises the accuracy of the model. Including screws could potentially make the femur more resistant to bending forces. Additionally, the simulated walking in the model only covers a limited range of motions, which may not capture movements that apply significant rotational force on the femur.[51]. Certain movements, such as biking, climbing stairs, standing from a chair, and squatting, can exert more force perpendicular to the mechanical axis of the femur, generating larger moments. These movements could potentially cause extreme stress and strain on specific areas of the femur. However, this would need to be tested in a model that incorporates a wider range of motions.

The model incorporating screws is limited due to the used material properties. Due to some technical limitations the femur was considered uniform. This severely simplifies the model. This model was only meant to show the possible interaction between the stress of the hinge and screws.

4.9. Future research

No definitive conclusion has been reached regarding the difference between medial open wedge DFO and lateral open wedge DFO. While it can be theorized that this difference may be due to a material discrepancy based on findings from this study and other literature reporting high incidences of hinge fractures using lateral hinges, further investigation is needed to confirm this hypothesis. Initially, this thesis focused on the assumption of differences in tension and compression between the two hinges, which was found to be untrue. Although the created models could be utilized for further analyses, they were not specifically tailored for this purpose. New technologies like XFEM could be explored in future research, but this would necessitate the development of new models to accommodate these advancements.

For future studies, conducting in vivo experiments would be intriguing. Ideally, this would involve multiple cadaver femurs undergoing both lateral and medial open wedge DFO procedures, followed by simulated walking motions. This would provide clarity regarding the location and timing of failure during both state 1 and state 2. Comparisons between the created models and in vivo experiments

could validate the conclusions drawn from this research. Additionally, testing various hinge sizes in vivo could verify the optimal hinge size identified in this thesis.

While many papers identify a lateral hinge as more prone to hinge fractures, a comparison of the material properties of hinges from both lateral and medial open wedge DFO procedures would be valuable. However, no literature comparing the material properties of the femur in these locations has been found thus far.

The effectiveness of drill holes was also considered in this study, but it did not yield promising results. However, the impact of a smaller hinge in step 2, considering the rounding of corners, remains unexplored. While existing literature suggests that a hinge that is too small may lead to instability and potential hinge fractures, further investigation is warranted in this area.

5. Conclusion

The goal of this study was to investigate the reasons for the incidence of hinge fractures (HF) in open wedge distal femoral osteotomy (DFO) on both the lateral and medial sides. However, no conclusive reason for the observed difference was found. The initial hypothesis, which suggested that the hinge would be under tension during medial open wedge DFO, was rejected. Additionally, existing literature indicates a significantly higher incidence of HF in medial closed wedge osteotomy, suggesting a potential difference in material properties, specifically the anisotropic properties of bone in different locations. Further research is needed to explore this aspect.

Based on the findings of this study, a 10 mm hinge for femoral osteotomies appears to be optimal, considering both the opening and loading of the osteotomy gap. The angle of the osteotomy plane was found to have a minimal impact on stress and strain.

While drill holes could potentially increase the size of correction until a fracture occurs, the proposed method for creating drill holes may have limited effectiveness. In cases of large corrections or patients with a high fracture probability, drill holes in the currently proposed manner may not be sufficient to prevent fractures. Therefore, alternative approaches to preventing HF in such cases may need to be explored.

The creation of patient-specific finite element models was demonstrated to be feasible. However, the usefulness of these models may be limited by the assumptions that need to be made about the material properties of bone. Further refinement of these models and validation against clinical data may enhance their utility in predicting and preventing HF in DFO procedures.

References

[1] D. J. Hunter, L. March, and M. Chew, “Osteoarthritis in 2020 and beyond: a Lancet Commission,” *The Lancet*, vol. 396, no. 10264. pp. 1711–1712, 2020, doi: 10.1016/S0140-6736(20)32230-3.

[2] N. van Egmond, *Joint Preservation of Unicompartmental Knee Osteoarthritis*. 2018.

[3] A. A. Najefi, K. Malhotra, and A. Goldberg, “Mechanical and anatomical axis of the lower limb in total ankle arthroplasty,” *Foot*, 2020, doi: 10.1016/j.foot.2020.101666.

[4] L. Sharma *et al.*, “NIH Public Access,” vol. 69, no. 11, pp. 1940–1945, 2011, doi: 10.1136/ard.2010.129742.Varus.

[5] A. Chang *et al.*, “Frequency of varus and valgus thrust and factors associated with thrust presence in persons with or at higher risk of developing knee osteoarthritis,” *Arthritis and Rheumatism*, vol. 62, no. 5. pp. 1403–1411, 2010, doi: 10.1002/art.27377.

[6] T. Griffin, N. Rowden, D. Morgan, R. Atkinson, P. Woodruff, and G. Maddern, “Unicompartmental knee arthroplasty for the treatment of unicompartmental osteoarthritis: A systematic study,” *ANZ J. Surg.*, vol. 77, no. 4, pp. 214–221, 2007, doi: 10.1111/j.1445-2197.2007.04021.x.

[7] L. Gao *et al.*, “Advances in modern osteotomies around the knee: Report on the Association of Sports Traumatology, Arthroscopy, Orthopaedic surgery, Rehabilitation (ASTAOR) Moscow International Osteotomy Congress 2017,” *J. Exp. Orthop.*, vol. 6, no. 1, 2019, doi: 10.1186/s40634-019-0177-5.

[8] J. Chahla *et al.*, “Opening- and Closing-Wedge Distal Femoral Osteotomy: A Systematic Review of Outcomes for Isolated Lateral Compartment Osteoarthritis,” *Orthop. J. Sport. Med.*, vol. 4, no. 6, pp. 1–8, 2016, doi: 10.1177/2325967116649901.

[9] G. Puddu, M. Cipolla, G. Cerullo, V. Franco, and E. Giannì, “Which osteotomy for a valgus knee?,” *Int. Orthop.*, vol. 34, no. 2 SPECIAL ISSUE, pp. 239–247, 2010, doi: 10.1007/s00264-009-0820-3.

[10] G. Vena, S. D’Adamio, and A. Amendola, “Complications of osteotomies about the knee,” *Sports Medicine and Arthroscopy Review*. 2013, doi: 10.1097/JSA.0b013e3182900720.

[11] R. Takeuchi *et al.*, “Fractures around the lateral cortical hinge after a medial opening-wedge high tibial osteotomy: A new classification of lateral hinge fracture,” *Arthrosc. - J. Arthrosc. Relat. Surg.*, 2012, doi: 10.1016/j.arthro.2011.06.034.

[12] P. W. Winkler *et al.*, “A hinge position distal to the adductor tubercle minimizes the risk of hinge fractures in lateral open wedge distal femoral osteotomy,” *Knee Surgery, Sport. Traumatol. Arthrosc.*, 2020, doi: 10.1007/s00167-020-06244-6.

[13] R. Takeuchi *et al.*, “Fractures around the lateral cortical hinge after a medial opening-wedge high tibial osteotomy: A new classification of lateral hinge fracture,” *Arthrosc. - J. Arthrosc. Relat. Surg.*, vol. 28, no. 1, pp. 85–94, 2012, doi: 10.1016/j.arthro.2011.06.034.

[14] R. Nakamura *et al.*, “The validity of the classification for lateral hinge fractures in open wedge high tibial osteotomy,” *Bone Jt. J.*, 2015, doi: 10.1302/0301-620X.97B9.34949.

[15] D. K. Bae, C. H. Park, E. J. Kim, and S. J. Song, “Medial cortical fractures in computer-assisted closing-wedge high tibial osteotomy,” *Knee*, 2016, doi: 10.1016/j.knee.2015.12.008.

[16] K. T. Kang, Y. G. Koh, J. A. Lee, J. J. Lee, and S. K. Kwon, “Biomechanical effect of a lateral hinge fracture for a medial opening wedge high tibial osteotomy: Finite element study,” *J. Orthop. Surg. Res.*, vol. 15, no. 1, pp. 1–10, 2020, doi: 10.1186/s13018-020-01597-7.

[17] B. S. Miller, W. O. P. Dorsey, C. R. Bryant, and J. C. Austin, “The effect of lateral cortex disruption and repair on the stability of the medial opening wedge high tibial osteotomy,” *Am. J. Sports Med.*, vol. 33, no. 10, pp. 1552–1557, 2005, doi: 10.1177/0363546505275488.

[18] J. H. Kim, D. kyung Lee, and Y. B. Park, “Computed Tomography Detects Hinge Fractures After Medial Opening Wedge High Tibial Osteotomy: A Systematic Review,” *Arthrosc. - J. Arthrosc. Relat. Surg.*, vol. 37, no. 4, pp. 1337–1352, 2021, doi: 10.1016/j.arthro.2020.11.031.

[19] E. Dessyn *et al.*, “Adding a protective K-wire during opening high tibial osteotomy increases lateral hinge resistance to fracture,” *Knee Surgery, Sport. Traumatol. Arthrosc.*, vol. 28, no. 3, pp. 751–758, 2020, doi: 10.1007/s00167-019-05404-7.

[20] T. W. Kim, M. C. Lee, J. H. Cho, J. S. Kim, and Y. S. Lee, “The Ideal Location of the Lateral Hinge in Medial Closing Wedge Osteotomy of the Distal Femur: Analysis of Soft Tissue Coverage and Bone Density,” *Am. J. Sports Med.*, vol. 47, no. 12, pp. 2945–2951, 2019, doi: 10.1177/0363546519869325.

[21] U. Sigurdsen, O. Reikeras, and S. Erik, “The influence of compression on the healing of experimental tibial fractures,” vol. 42, pp. 1152–1156, 2011, doi: 10.1016/j.injury.2010.08.018.

[22] K. J. H. Newman, B. Ollivere, K. Kojima, R. Handley, N. D. Rossiter, and C. G. Moran, “A unified theory of bone healing and nonunion BHN THEORY,” pp. 884–891, 1978, doi: 10.1302/0301-620X.98B7.36061.

[23] A. Boström, A. K. Amin, G. J. Macpherson, P. Pankaj, and C. E. H. Scott, “Hinge location and apical drill holes in opening wedge high tibial osteotomy: A finite element analysis,” *J. Orthop. Res.*, vol. 39, no. 3, pp. 628–636, 2021, doi: 10.1002/jor.24704.

[24] V. A. Carranza, J. Reeves, A. Getgood, and T. A. Burkhart, “Development and validation of a finite element model to simulate the opening of a medial opening wedge high tibial osteotomy,” *Comput. Methods Biomech. Biomed. Engin.*, vol. 22, no. 4, pp. 442–449, 2019, doi: 10.1080/10255842.2018.1563599.

[25] A. D. Kaze, S. Maas, A. Hoffmann, and D. Pape, “Mechanical strength assessment of a drilled hole in the contralateral cortex at the end of the open wedge for high tibial osteotomy,” 2017, doi: 10.1186/s40634-017-0098-0.

[26] H. Ogawa, K. Matsumoto, and H. Akiyama, “The prevention of a lateral hinge fracture as a complication of a medial opening wedge high tibial osteotomy,” *Bone Jt. J.*, 2017, doi: 10.1302/0301-620X.99B7.BJJ-2016-0927.R1.

[27] L. Grassi, S. P. Väänänen, M. Ristinmaa, J. S. Jurvelin, and H. Isaksson, “Corrigendum to ‘How accurately can subject-specific finite element models predict strains and strength of human femora? Investigation using full-field measurements’ (Journal of Biomechanics (2016) 49(5) (802–806), (S0021929016301865) (10.1016/j.jbiomech.2,” *J. Biomech.*, vol. 84, pp. 290–292, 2019, doi: 10.1016/j.jbiomech.2018.12.032.

[28] Z. Saghaei and A. Hashemi, “Effect of hinge length on the lateral cortex fracture in high tibia osteotomy: an XFEM study,” *Comput. Methods Biomech. Biomed. Engin.*, vol. 0, no. 0, pp. 1–9, 2021, doi: 10.1080/10255842.2021.1974419.

[29] S. B. Han, J. H. Choi, A. Mahajan, and Y. S. Shin, “Incidence and Predictors of Lateral Hinge Fractures Following Medial Opening-Wedge High Tibial Osteotomy Using Locking Plate System:

Better Performance of Computed Tomography Scans," *J. Arthroplasty*, 2019, doi: 10.1016/j.arth.2019.01.026.

[30] D. Dragomir-daescu, A. Nassr, and M. J. Yaszemski, "Quantitative Computed Tomography Protocols Affect Material Mapping and Quantitative Computed Finite-Element Analysis Predicted Stiffness," vol. 138, no. September, pp. 1–7, 2016, doi: 10.1115/1.4034172.

[31] E. A. Zimmermann and R. O. Ritchie, "Bone as a Structural Material," pp. 1287–1304, 2015, doi: 10.1002/adhm.201500070.

[32] R. Warkhedkar, "Analysis of Hounsfield Unit of Human Bones for Strength Evaluation ScienceDirect Analysis of Hounsfield Unit of Human Bones for Strength Evaluation," no. December 2015, 2014, doi: 10.1016/j.mspro.2014.07.065.

[33] F. Buenger, Y. Sakr, N. Eckardt, C. Senft, and F. Schwarz, "Correlation of quantitative computed tomography derived bone density values with Hounsfield units of a contrast medium computed tomography in 98 thoraco - lumbar vertebral bodies," *Arch. Orthop. Trauma Surg.*, no. 0123456789, 2021, doi: 10.1007/s00402-021-04184-5.

[34] B. L. S. Ang *et al.*, "The effect of specimen geometry on the mechanical behavior of trabecular bone specimens," *Solid State Phenom.*, vol. 185, no. 4, pp. 129–132, 2012, doi: 10.4028/www.scientific.net/SSP.185.129.

[35] L. Peng, J. Bai, X. Zeng, and Y. Zhou, "Comparison of isotropic and orthotropic material property assignments on femoral finite element models under two loading conditions," *Med. Eng. Phys.*, vol. 28, no. 3, pp. 227–233, 2006, doi: 10.1016/j.medengphy.2005.06.003.

[36] A. Bansiddhi and D. C. Dunand, *Titanium and NiTi foams for bone replacement*. Woodhead Publishing Limited, 2014.

[37] H. Kainz *et al.*, "A multi-scale modelling framework combining musculoskeletal rigid-body simulations with adaptive finite element analyses, to evaluate the impact of femoral geometry on hip joint contact forces and femoral bone growth," *PLoS One*, vol. 15, no. 7 July, pp. 1–18, 2020, doi: 10.1371/journal.pone.0235966.

[38] and A. I. H. Elise F. Morgan, Ginu U. Unnikrisnan, "HHS Public Access," *Annu. Rev. Biomed. Eng.*, vol. 20, no. 10, pp. 119–143, 2018, doi: 10.1146/annurev-bioeng-062117-121139.Bone.

[39] J. W. Seo *et al.*, "Finite element analysis of the femur during stance phase of gait based on musculoskeletal model simulation," *Biomed. Mater. Eng.*, vol. 24, no. 6, pp. 2485–2493, 2014, doi: 10.3233/BME-141062.

[40] J. Seo, J. Choi, D. Kang, J. Bae, and G. Tack, "Differences in Stress and Total Deformation Due to Muscle Attachment to the Femur," *World Acad. Sci. Eng. Technol.*, vol. 63, no. 3, pp. 54–57, 2012.

[41] U. Wolfram and J. Schwiedrzik, "Post-yield and failure properties of cortical bone," *Nat. Publ. Gr.*, vol. 5, no. March, pp. 1–10, 2016, doi: 10.1038/bonekey.2016.60.

[42] K. Fujita, T. Sawaguchi, K. Goshima, K. Shigemoto, and S. Iwai, "Influence of lateral hinge fractures on biplanar medial closing - wedge distal femoral osteotomy for valgus knee : a new classification of lateral hinge fracture," *Arch. Orthop. Trauma Surg.*, no. 0123456789, 2021, doi: 10.1007/s00402-021-04212-4.

[43] A. K. Gangavalli and C. O. Nwachuku, "Management of Distal Femur Fractures in Adults. An Overview of Options," *Orthop. Clin. North Am.*, vol. 47, no. 1, pp. 85–96, 2016, doi: 10.1016/j.ocl.2015.08.011.

[44] J. E. Wiss D, Watson JT, *Rockwood and Green's fractures in adults*, 4th ed. Pennsylvania: Lippincott Williams and Wilkins, 1996.

[45] Y. Morita, S. Kuriyama, T. Maeda, S. Nakamura, K. Nishitani, and H. Ito, "Hinge fractures reaching the tibial plateau can be caused by forcible opening of insufficient posterior osteotomy during open - wedge high tibial osteotomy," *Knee Surgery, Sport. Traumatol. Arthrosc.*, no. 0123456789, 2021, doi: 10.1007/s00167-021-06816-0.

[46] M. J. Mirzaali *et al.*, "Mechanical properties of cortical bone and their relationships with age , gender , composition and microindentation properties in the elderly," *Bone*, vol. 93, pp. 196–211, 2016, doi: 10.1016/j.bone.2015.11.018.

[47] S. Poelert, E. Valstar, H. Weinans, and A. A. Zadpoor, "Patient-specific finite element modeling of bones," *Proc. Inst. Mech. Eng. Part H J. Eng. Med.*, vol. 227, no. 4, pp. 464–478, 2013, doi: 10.1177/0954411912467884.

[48] L. Duchemin, V. Bousson, C. Raossanaly, and C. Bergot, "Prediction of mechanical properties of cortical bone by quantitative computed tomography," vol. 30, pp. 321–328, 2008, doi: 10.1016/j.medengphy.2007.04.008.

[49] S. Kamalian, M. H. Lev, and R. Gupta, *Computed tomography imaging and angiography – principles*, 1st ed., vol. 135. Elsevier B.V., 2016.

[50] D. Fellow, "IRC-18-65 IRCOBI conference 2018," pp. 388–398, 2018.

[51] S. J. G. Taylor, P. S. Walker, J. S. Perry, S. R. Cannon, and R. Woledge, "The forces in the distal femur and the knee during walking and other activities measured by telemetry," *J. Arthroplasty*, vol. 13, no. 4, pp. 428–437, 1998, doi: 10.1016/S0883-5403(98)90009-2.

[52] P. Biggs, "Can Gaming Technology Be Used for Human Motion Analysis ?," *MMM – Med. Eng.*, no. March, 2012.